Resource

Cell

A Spatiotemporal Organ-Wide Gene Expression and Cell Atlas of the Developing Human Heart

Graphical Abstract

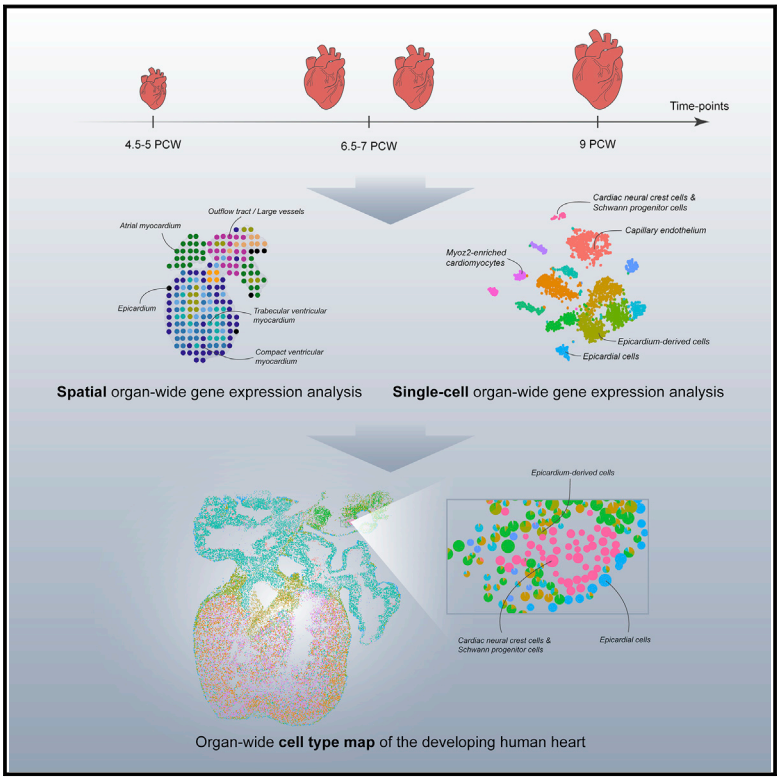

Highlights

- Profiled spatiotemporal gene expression patterns in human cardiogenesis
- Mapped cell-type distribution and spatial organization in the human embryonic heart
- Thoroughly analyzed roles of diverse cell types in cardiac development
- A publicly available web resource of the human embryonic heart

Authors

Michaela Asp, Stefania Giacomello, Ludvig Larsson, ..., Mats Nilsson, Christer Sylvén, Joakim Lundeberg

Correspondence

michaela.asp@scilifelab.se (M.A.), joakim.lundeberg@scilifelab.se (J.L.)

In Brief

The gene expression landscape of human heart development is explored at single-cell resolution with spatial transcriptomic approaches to construct a 3D organ-wide atlas.

Asp et al., 2019, Cell *179*, 1647–1660
December 12, 2019
https://doi.org/10.1016/j.cell.2019.11.025

CellPress

Resource

Cell

A Spatiotemporal Organ-Wide Gene Expression and Cell Atlas of the Developing Human Heart

Michaela Asp,[1,13,*] Stefania Giacomello,[1,2,13] Ludvig Larsson,[1,14] Chenglin Wu,[3,14] Daniel Fürth,[4,14] Xiaoyan Qian,[3] Eva Wärdell,[5] Joaquin Custodio,[6] Johan Reimegård,[7] Fredrik Salmén,[8] Cecilia Österholm,[9] Patrik L. Ståhl,[1] Erik Sundström,[10] Elisabet Åkesson,[10] Olaf Bergmann,[11,12] Magda Bienko,[6] Agneta Månsson-Broberg,[5] Mats Nilsson,[3] Christer Sylvén,[5] and Joakim Lundeberg[1,15,*]

[1]Science for Life Laboratory, Department of Gene Technology, KTH Royal Institute of Technology, Stockholm, Sweden
[2]Department of Biochemistry and Biophysics, National Bioinformatics Infrastructure Sweden, Science for Life Laboratory, Stockholm University, Stockholm, Sweden
[3]Science for Life Laboratory, Department of Biochemistry and Biophysics, Stockholm University, Stockholm, Sweden
[4]Cold Spring Harbor Laboratory, Cold Spring Harbor, NY 11724, USA
[5]Department of Medicine, Karolinska Institutet, Huddinge, Sweden
[6]Science for Life Laboratory, Department of Medical Biochemistry and Biophysics, Karolinska Institutet, Stockholm, Sweden
[7]Department of Cell and Molecular Biology, National Bioinformatics Infrastructure Sweden, Science for Life Laboratory, Uppsala University, Uppsala, Sweden
[8]Hubrecht Institute-KNAW (Royal Netherlands Academy of Arts and Sciences) and University Medical Center Utrecht, Cancer Genomics Netherlands, Utrecht, the Netherlands
[9]Department of Molecular Medicine and Surgery, Karolinska Institutet, Stockholm, Sweden
[10]Department of Neurobiology, Care Sciences and Society, Karolinska Institutet, R&D Unit, Stockholms Sjukhem, Stockholm, Sweden
[11]Center for Regenerative Therapies Dresden, TU-Dresden, Dresden, Germany
[12]Karolinska Institutet, Cell and Molecular Biology, Stockholm, Sweden
[13]These authors contributed equally
[14]These authors contributed equally
[15]Lead Contact
*Correspondence: michaela.asp@scilifelab.se (M.A.), joakim.lundeberg@scilifelab.se (J.L.)
https://doi.org/10.1016/j.cell.2019.11.025

SUMMARY

The process of cardiac morphogenesis in humans is incompletely understood. Its full characterization requires a deep exploration of the organ-wide orchestration of gene expression with a single-cell spatial resolution. Here, we present a molecular approach that reveals the comprehensive transcriptional landscape of cell types populating the embryonic heart at three developmental stages and that maps cell-type-specific gene expression to specific anatomical domains. Spatial transcriptomics identified unique gene profiles that correspond to distinct anatomical regions in each developmental stage. Human embryonic cardiac cell types identified by single-cell RNA sequencing confirmed and enriched the spatial annotation of embryonic cardiac gene expression. *In situ* sequencing was then used to refine these results and create a spatial subcellular map for the three developmental phases. Finally, we generated a publicly available web resource of the human developing heart to facilitate future studies on human cardiogenesis.

INTRODUCTION

The heart is the first solid organ in the human embryo that becomes functional. It originates from the mesoderm and develops into the cardiac tube, which starts to beat around 21 days after conception (Sylva et al., 2014; Meilhac and Buckingham, 2018). The cardiac tube then loops, forming the four individual cardiac chambers (i.e., left and right atria and left and right ventricles) and the epicardium after about 30 days. Subsequently, the outflow tract (OFT) differentiates, and the outer part of the ventricular myocardium transforms into the compact myocardium and the septum. Eventually, the OFT divides into the aorta and the pulmonary artery, and most of the cardiac compartments are complete by the end of the first trimester. These complex events are the result of intricate and well-timed gene expression interactions related to the spatial and functional programs acting in each part of the developing heart.

Rapid advancements in single-cell RNA sequencing (scRNA-seq) technologies have enabled the use of single-cell transcriptional profiling to explore cellular heterogeneity within the heart, advancing our knowledge of cardiac differentiation processes. For example, studies on embryonic (DeLaughter et al., 2016; Li et al., 2016; Lescroart et al., 2018) and adult (Gladka et al., 2018) murine hearts have provided cell-specific findings that could not have been attained using tissue homogenates. Moreover, prior knowledge of the spatial locations of cardiac cells has been pivotal to revealing both chamber-specific genes and distinct spatiotemporal cardiomyocyte populations in the embryonic mouse heart (DeLaughter et al., 2016; Li et al., 2016). However, there are differences between murine and human cardiac development; temporal scRNA-seq studies have revealed human-specific

genes that are expressed during development (Cui et al., 2019) and important for differentiation (Sahara et al., 2019).

A common feature to transcriptome-wide scRNA-seq studies is that they do not resolve the spatial patterns of cardiac gene expression. We therefore need alternative methods that can provide positional information on the different cell types involved in the process, which is necessary for a comprehensive understanding of developmental dynamics (Regev et al., 2017). Several technologies for studying spatial gene expression patterns have been reported. These can be divided into targeted methods (Ke et al., 2013; Chen et al., 2015; Wang et al., 2018; Eng et al., 2019), which require prior knowledge about the genes of interest, and untargeted methods (Junker et al., 2014; Lee et al., 2014; Lovatt et al., 2014; Ståhl et al., 2016; Rodriques et al., 2019; Vickovic et al., 2019), which do not.

Given the complexity and incomplete understanding of human cardiac development, we considered it important to establish a molecular approach that enables simultaneous analysis of spatial cardiac gene expression patterns and cellular heterogeneity. We hypothesized that such an approach could be developed using spatial transcriptomics (ST) (Ståhl et al., 2016; Salmén et al., 2018), scRNA-seq (Zheng et al., 2017), and *in situ* sequencing (ISS) (Ke et al., 2013; Qian et al., 2019). ST is an untargeted technology that determines the quantitative spatial distribution of polyadenylated transcripts in a tissue section using barcoded oligo-dT arrays and standard histological brightfield imaging. It generates data-driven spatial maps and has broad applicability (Giacomello et al., 2017; Giacomello and Lundeberg, 2018; Lundmark et al., 2018). Among other things, it has been used to analyze organs including the brain (Ståhl et al., 2016; Salmén et al., 2018) and the adult human heart (Asp et al., 2017), as well as neurodegeneration (Maniatis et al., 2019). Conversely, ISS is a targeted approach that uses padlock probes and rolling circle amplification in tissue sections to target known genes (Ke et al., 2013; Qian et al., 2019). It facilitates analysis with subcellular resolution to confirm regional markers and cell type identifications based on ST and scRNA-seq.

Here, we present a spatiotemporal atlas that systematically describes the spatial archetypes and cellular heterogeneity of the developing human heart at three developmental stages in the first trimester: 4.5–5, 6.5, and 9 post-conception weeks (PCW) (Figure 1). We created this resource by exploiting the spatial exploratory power of ST, the deconvolution capabilities of scRNA-seq, and the subcellular targeted accuracy of ISS. Finally, we visualized our results by integrating the spatial information to generate three-dimensional (3D) transcriptional maps.

RESULTS

Spatiotemporal Gene Expression Dynamics during Human Heart Development

We initially obtained a spatiotemporal overview of human heart development by immunohistochemical (IHC) staining of tissue sections from human embryonic cardiac samples collected at 4.5–5, 6.5, and 9 PCW (Figures 2A–2C). This revealed that the free walls and septa of the left and right ventricles, and the left and right atria (*TNNT2*), consist of compact and trabecular ventricular myocardium at all time points. Additionally, smooth muscle actin (*ACTA2*) staining showed that the formation of the aorta and pulmonary artery had begun in the 4.5–5 PCW heart and had advanced in the 6.5 and 9 PCW hearts. DAPI (4,6-diamidino-2-phenylindole) staining revealed a thin epicardial border enveloping the heart at all three time points. However, the atrioventricular (AV) subepicardial mesenchyme, from which the coronary arteries form (*ACTA2*), was only visible at the upper end of the AV sulcus at the 6.5 and 9 PCW stages. Finally, at the end of the pericardial cavity, where the large arteries pass into the mediastinum, we observed a considerable amount of mediastinal tissue with pulmonary veins (*ACTA2*) that was only visible in the 6.5 and 9 PCW hearts. In summary, IHC staining clearly revealed spatiotemporal protein expression patterns during human heart development. However, the analysis was limited by the use of a panel of preselected antibodies.

To expand our study in an unbiased manner, we used ST to explore global spatiotemporal gene expression dynamics during human heart development. Specifically, we collected four, nine, and six tissue sections along the dorsal-ventral axis from the 4.5–5, 6.5, and 9 PCW heart tissues, respectively (Figure S1A; Table S1A). The joint dataset consisted of a total pool of 3,115 individual spots (i.e., data points equivalent to microdissections containing ~30 cells each (Figures S1L–S1O) with an average of ~1,700 genes and ~3,800 unique transcripts per spot after filtering (Figures S1B and S1C). We examined similarities between technical replicates by determining Pearson correlations and found that all time points were comparable (Figures S1D–S1G) with regard to gene expression levels. To investigate the biological differences between the three time points, we calculated the gene expression correlation between the samples, revealing that the overall bulk gene expression patterns at all developmental stages were quite similar (Figures S1H–S1J). We then performed dimensionality reduction and clustering on the joint spatial (spot) gene expression profiles of all three stages. We identified ten spatiotemporally conserved clusters (Figure 2D) and mapped the clustered spots back to their original coordinates in the tissue sections. Strikingly, the clusters corresponded to defined anatomical regions in all three hearts (Figures 2E–2G; see Data S1 at https://data.mendeley.com/datasets/zkzvyprd5z/draft?a=c3021f62-a7af-4824-b89d-d7fbfec67902). The main myocardial regions (clusters 0, 1, 2, 3, and 4) were shared across all time points and appeared to reflect the heart's growth because the numbers of spots in these clusters increased with age (Figure S1K). The OFT and larger vessels (cluster 5) were underrepresented in the 4.5–5 PCW tissue in comparison to the other two ages and were mainly represented by AV mesenchyme (cluster 6). Moreover, cavities with blood and immune cells (cluster 8) were only represented by spots from the 6.5 PCW tissue, which contained more blood than the other two hearts (see STAR Methods).

We performed differential gene expression (DGE) analysis between anatomical regions (Figure 2H; Table S2) and gene set enrichment analysis of each cluster's upregulated genes (Figure S2A). Gene ontology (GO) characteristics related to muscle contraction and development were detected across all

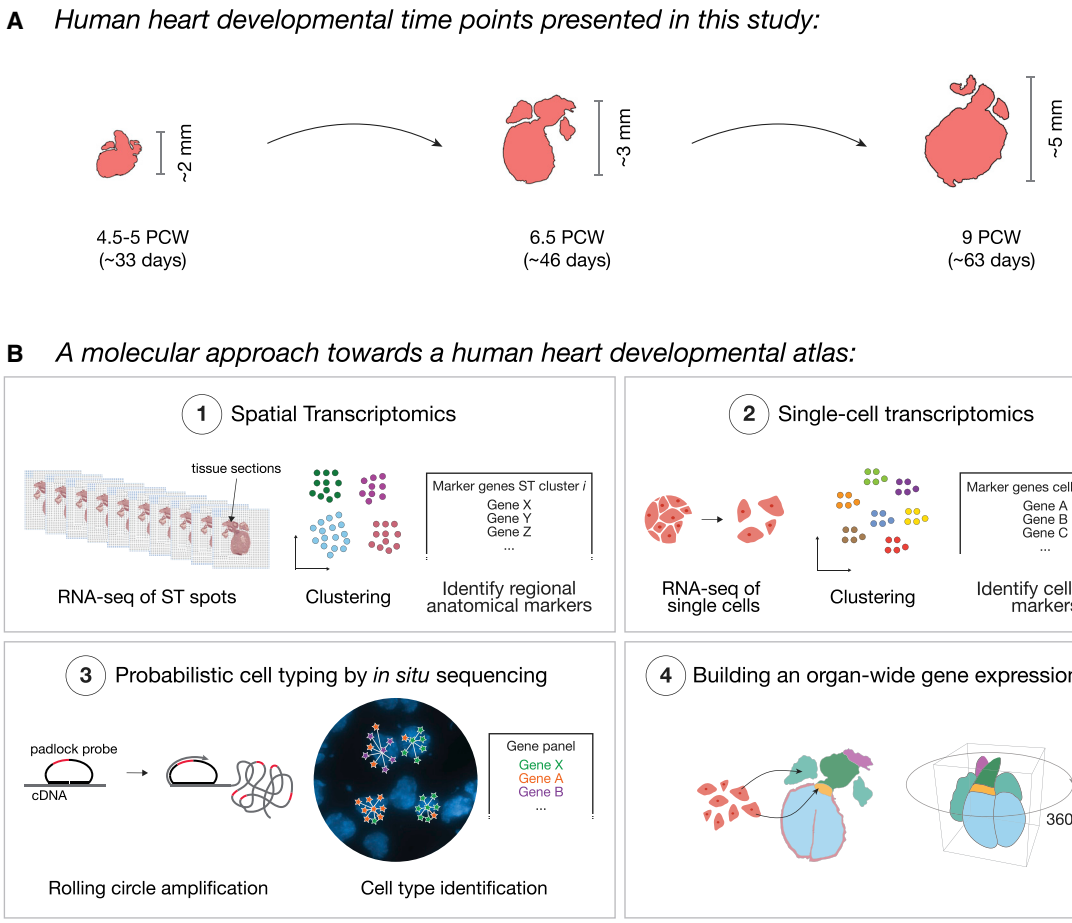

Figure 1. Overview of the Study

(A) Developmental stages of three human cardiac tissues included in this study. Days are defined as days post-conception.

(B) Overview of the molecular approach presented in this study; the steps are as follows: (1) explore transcriptome-wide spatiotemporal patterns in the three hearts by ST, (2) dissect cell type heterogeneity of the heart at intermediate time point by scRNA-seq, (3) target key genes at subcellular resolution by ISS, and (4) generate 3D gene expression atlas.

myocardial clusters (0, 1, 2, 3, and 4), whereas the compact myocardium (cluster 0) was enriched in metabolism. The three trabecular clusters (1, 2, and 3) could be distinguished by their enrichment in conduction (clusters 1 and 2) and oxidative metabolism (cluster 3) (Figure S2A). In addition, cluster 2 exhibited differential expression of *MB* and *NPPA* (Figure 2H), which is associated with enhanced oxygen transport and endocrine activity (Lin et al., 1990). Therefore, the different trabecular myocardial clusters may correspond to distinct components of the trabeculi, such as wall-related, papillary muscle, or Purkinje fibers. The atrial myocardium (cluster 4) also displayed differential expression of *NPPA* (indicating endocrine activity) (Figure 2H), as well as genes related to conduction and heart rate regulation (Figure S2A). On the other hand, the OFT, the AV and mediastinal mesenchyme, and the epicardium (clusters 5, 6, 7, and 9) exhibited similar GO characteristics; they were enriched in terms related to the extracellular matrix and different degrees of vasculature and artery morphogenesis. Clusters 5, 6, and 7 were also enriched in characteristics related to heart valve and septum development (Figure S2A). Cluster 9 demonstrated expression of the epicardial markers *ALDH1A2* (Moss et al., 1998), *LRP2*, and *ITLN1*, and the epicardium and epicardium-derived cell (EPDC) marker *TBX18* (Cai et al., 2008; Wu et al., 2013) (Figure 2H; Table S2). A deeper exploration of the OFT cluster (cluster 5), which was detected primarily in samples from the two later developmental time points (6.5 and 9 PCW), revealed enrichment in fibroblast-related extracellular matrix gene expression (such as *ELN*, *SPARC*, and *OGN*) and the expression of smooth muscle-related genes such as *ACTA2* and *MYH11* (Figure 2H). These markers were expressed much less strongly in the distal part of the AV mesenchyme of the earlier 4.5–5 PCW tissue (Figure S2B), implying that while the OFT grows out of the AV mesenchyme, its muscularization and the formation of the larger vessels start developing more distally, where cardiac neural crest cells are found.

In general, these results suggest that within the studied time window (4.5-9 PCW), spatial gene expression is established early on and maintained throughout embryonic development, and that differences in gene expression between regions within the heart are more pronounced than those between time points.

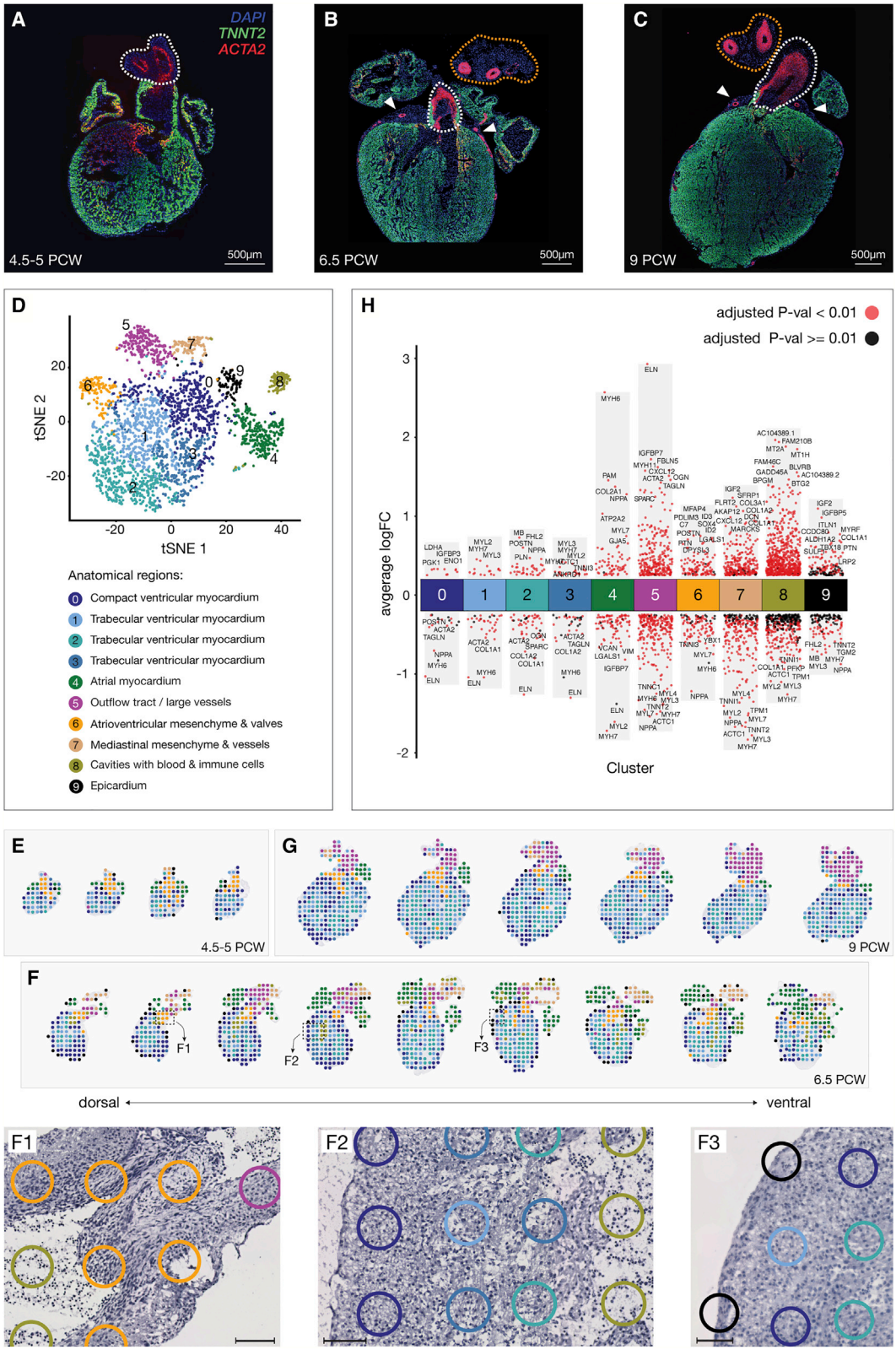

(legend on next page)

Single-Cell Gene Expression Analysis of a 6.5–7 PCW Human Embryonic Heart

Because the ST spots contained gene expression signatures of ~30 cells on average (Figures S1L–S1O), we used scRNA-seq to dissect the gene expression heterogeneity of the 6.5 PCW tissue sample. Specifically, we examined a biological replicate (i.e., a second human embryonic cardiac tissue sample) of the 6.5–7 PCW sample because IHC staining indicated that the intermediate time point displayed anatomical features identified in the other two stages. The tissue was dissected into two regionally distinct fractions: one containing the OFT, the AV structures, and most of the atria and another containing the ventricles. This facilitated cellular dissociation while retaining information on whether the studied cells derived from the upper or lower part of the heart.

Using a 10X Genomics Chromium workstation, we generated 3,717 single-cell transcriptional profiles with an average of ~2,900 genes and ~11,000 unique transcripts per cell after quality trimming and filtering (Figures S3A–S3C; Table S1B).

To verify that this 6.5 PCW heart sample could be considered a biological replicate of the 6.5 PCW heart analyzed by ST, we compared the two samples' scRNA-seq and ST bulk gene expression similarities. A strong correlation was observed (r = 0.93; Figure 3A), justifying the biological comparison. We identified 18,046 genes shared between the two 6.5 PCW samples, while 2,027 were expressed only in the scRNA-seq sample and 1,174 were unique to the ST sample. Most of the genes uniquely detected in the ST sample were Y-linked genes (e.g. *TTTY14*, *TTTY15*, and *ZFY*), a result of different gender representation. This was further confirmed by the overexpression of the *XIST* gene in the scRNA-seq sample (Ray et al., 1997). Furthermore, when inspecting genes found only in the scRNA-seq sample, we observed genes related to immune responses (e.g. *FCGR2B* and *IL6*) and cellular proliferation and apoptosis (*IL1B*), indicating the activation of these processes during the dissociation step prior to single-cell library preparation.

Finally, we performed dimensionality reduction and clustering of the gene expression profiles of the two single-cell fractions and identified 15 cell clusters (Figure 3B), which we categorized into cell types based on marker gene expression (Table S3). We were able to identify known cardiac cell types, ranging from cardiomyocytes and fibroblasts to smooth muscle and endothelial cells. Moreover, we detected three types of cardiomyocytes, cardiac neural crest cells, Schwann progenitor cells, epicardial cells, EPDCs (Masters and Riley, 2014; Sylva et al., 2014), two types of endothelial cells, and four types of fibroblast-like cell types. Certain cell clusters were only detected in cell fraction (i) (Figure 3C), suggesting rich cell diversity in the upper part of the heart, which contains the OFT, the main part of the atria, the AV sub-epicardial mesenchyme, the valvular apparatus, and the mediastinal tissue with the pulmonary veins.

Creating a Cellular Gene Expression Map of the Developing Heart

To clarify the spatial distribution of the different cell types present in the human embryonic heart and the heterogeneity of its spatial domains, we exploited the subcellular spatial resolution of ISS by applying it to the three cardiac tissues analyzed by ST, enabling a spatiotemporal analysis of gene expression with single-cell resolution. To this end, we designed a gene panel that leveraged information from the ST and scRNA-seq analysis of the two matched 6.5–7 PCW biological samples. Specifically, half of the initial gene panel consisted of key spatial marker genes identified by ST, and the other half consisted of marker genes for each scRNA-seq cluster (except for immune cells) to dissect cell-type heterogeneity. We subsequently added genes previously reported to be important for cardiac development, resulting in a final panel of 69 genes (Tables S4A and S4B). Upon re-clustering the scRNA-seq dataset using only the 69 genes included in the panel, we were able to assign the majority of cells to their original clusters; the sole exception was cluster 13, where the panel contained no specific marker genes (Figures S4A–S4C). We performed ISS experiments on all three hearts in replicates (Table S4C; Figure S4D) and observed high correlation within temporal stages (R^2 = 0.85–0.99). We also cross-validated three ISS gene probe results using single-molecule RNA fluorescence *in situ* hybridization (smFISH) (Figure 4), which generated patterns similar to those observed by sequencing.

Finally, we used the power of ISS and the pciSeq approach (Qian et al., 2019) to create a comprehensive probabilistic spatial cell map of the scRNA-seq defined cell types identified in the 6.5-7 PCW embryonic human heart (Figure 5). In addition to the spatial location, the cell mapping algorithm leverages scRNA-seq data to assign reads to individual cells (Figures 5A, 5C, and 5E). Our spatial map comprised 20,920 single cells (i.e. 76.2% of total number of cells in the tissue section) that were successfully assigned to the cell types defined by scRNA-seq (not including erythrocytes and immune cells, which were excluded from the analysis) (Figures 5B and 5D). The spatial cell mapping confirmed the spatial

Figure 2. Global Spatiotemporal Analysis of Three Cardiac Developmental Stages

(A–C) Immunostainings of tissue sections from the 4.5–5 PCW (A), 6.5 PCW (B), and 9 PCW (C) heart samples, showing their overall anatomical landscapes. Spatial protein expression of troponin T (*TNNT2*) is identified in the left and right ventricles, as well as the left and right atria. Spatial protein expression of aortic smooth muscle actin (*ACTA2*) is displayed in the OFT, showing the gradual formation of the aorta and pulmonary artery in the three stages (indicated by the white dashed lines). *ACTA2* is also seen in the coronary arteries located in the subepicardial mesenchyme in the 6.5 PCW and 9 PCW time points (indicated by the white arrows). Mediastinal tissue containing pulmonary veins (*ACTA2*) is only seen in the later stages (indicated by the orange dashed lines). Scale bars, 500 μm.

(D) Dimensionality reduction and clustering of 3,115 spots from 19 tissue sections of 4.5–5, 6.5, and 9 PCW human embryonic hearts. Each cluster's annotated anatomical region is indicated below.

(E–G) Mapping of data points from all ten clusters to their spatial positions show that clusters are localized to distinct histological regions. Magnified images of the histological structures are shown in F1–F3. Scale bars, 100 μm.

(H) Differential gene expression analysis showing up- and down-regulated genes across all ten clusters. An adjusted p value < 0.01 is indicated in red, while an adjusted p value ≥ 0.01 is indicated in black.

(A–C) and (E–G) Figures contain tiled images to cover the entire tissue.

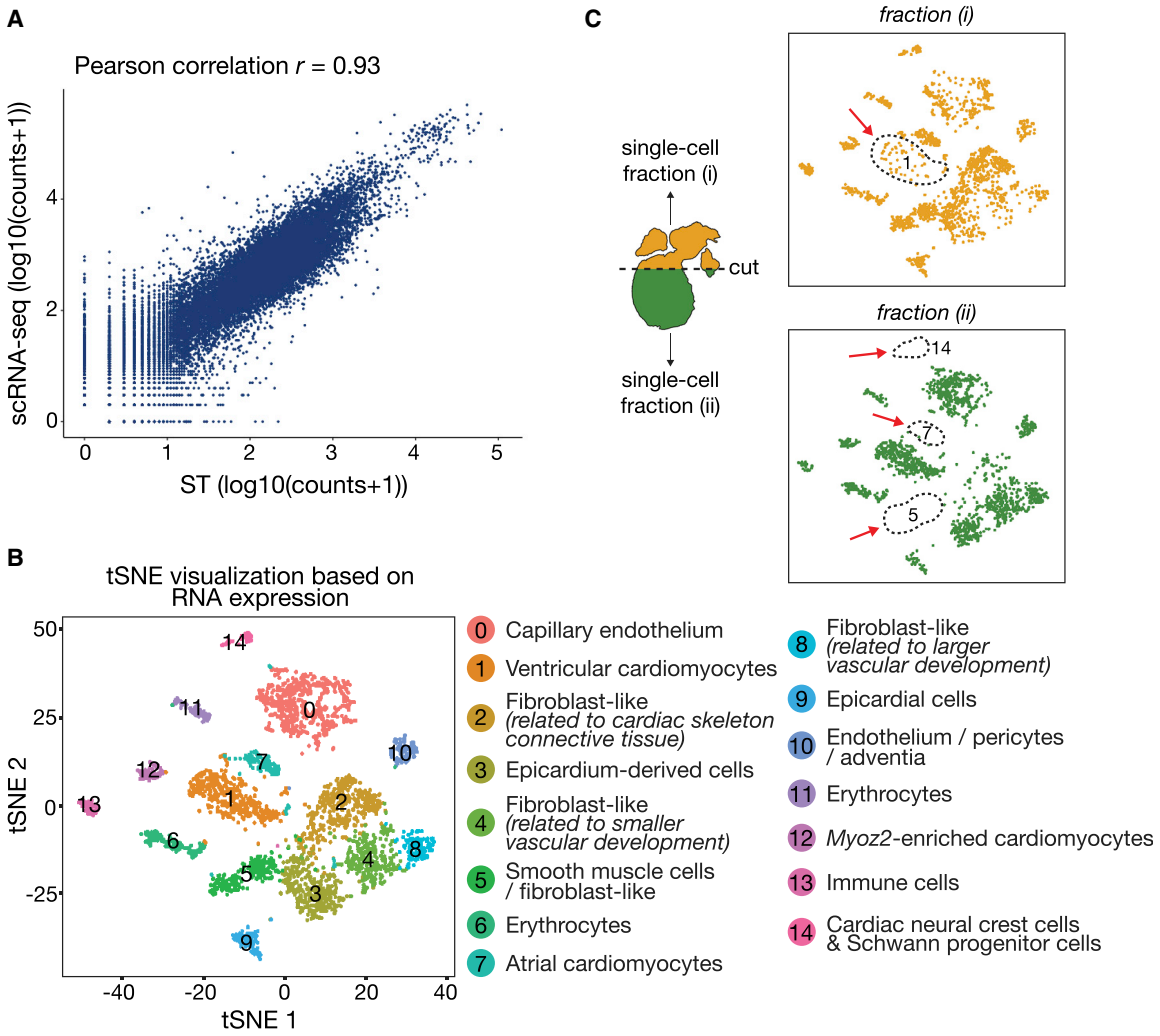

Figure 3. Single-Cell Analysis of a 6.5–7 PCW Human Embryonic Heart

(A) Scatterplot showing Pearson correlation between aggregated gene counts from cells of the 6.5–7 PCW heart sample and aggregated gene counts from spots of the 6.5 PCW heart sample.

(B) Dimensionality reduction and clustering of 3,717 single cells from the 6.5–7 PCW heart colored by cluster affiliation. The identified cell types, which are annotated based on marker gene information, are indicated on the right.

(C) tSNE plot shown in (B) where cells are colored based on their origin in the respective two heart fractions obtained prior to cell dissociation. The dashed line in fraction (i) illustrates cluster 1 (ventricular cardiomyocytes), which is present to a considerable larger extent in fraction (ii). The dashed lines in fraction (ii) illustrate absent clusters 5, 7, and 14 (smooth muscle cells/fibroblast-like, atrial cardiomyocytes, and cardiac neural crest and Schwann progenitor cells), which are present in fraction (i).

distribution of the clusters predicted by ST and also resolved finer structures formed by different cell types located in close proximity to one-another.

Disentangling Cell-Type Similarities by Spatial Analysis

The ISS analysis revealed clear spatial gene expression patterns consistent with the ST and scRNA-seq results for the studied cell types in the 6.5–7 PCW hearts (with immune cells and erythrocytes excluded from the analysis). Examples of the congruence between the three technologies are presented in Figures 6A–6B and S5A. The ISS results allowed us to gain a deeper understanding of several scRNA-seq clusters by comparing scRNA-seq results with those for the corresponding spatial marker genes.

Notably, we identified two cell-type subpopulations within cluster 14: cardiac neural crest cells expressing *ISL1* (Engleka et al., 2012) and *STMN2* (Anderson and Axel, 1985; Groves et al., 1995; Burzynski et al., 2009) and Schwann progenitor cells (Petersen and Adameyko, 2017; Jessen and Mirsky, 2019) expressing *ALDH1A1* (Figure 6A). Both cell types were present in the mediastinal mesenchyme and the OFT, and Schwann progenitor cells were also detected towards the AV sub-epicardial mesenchyme. By analyzing the ISS patterns of these genes within the OFT at the three developmental

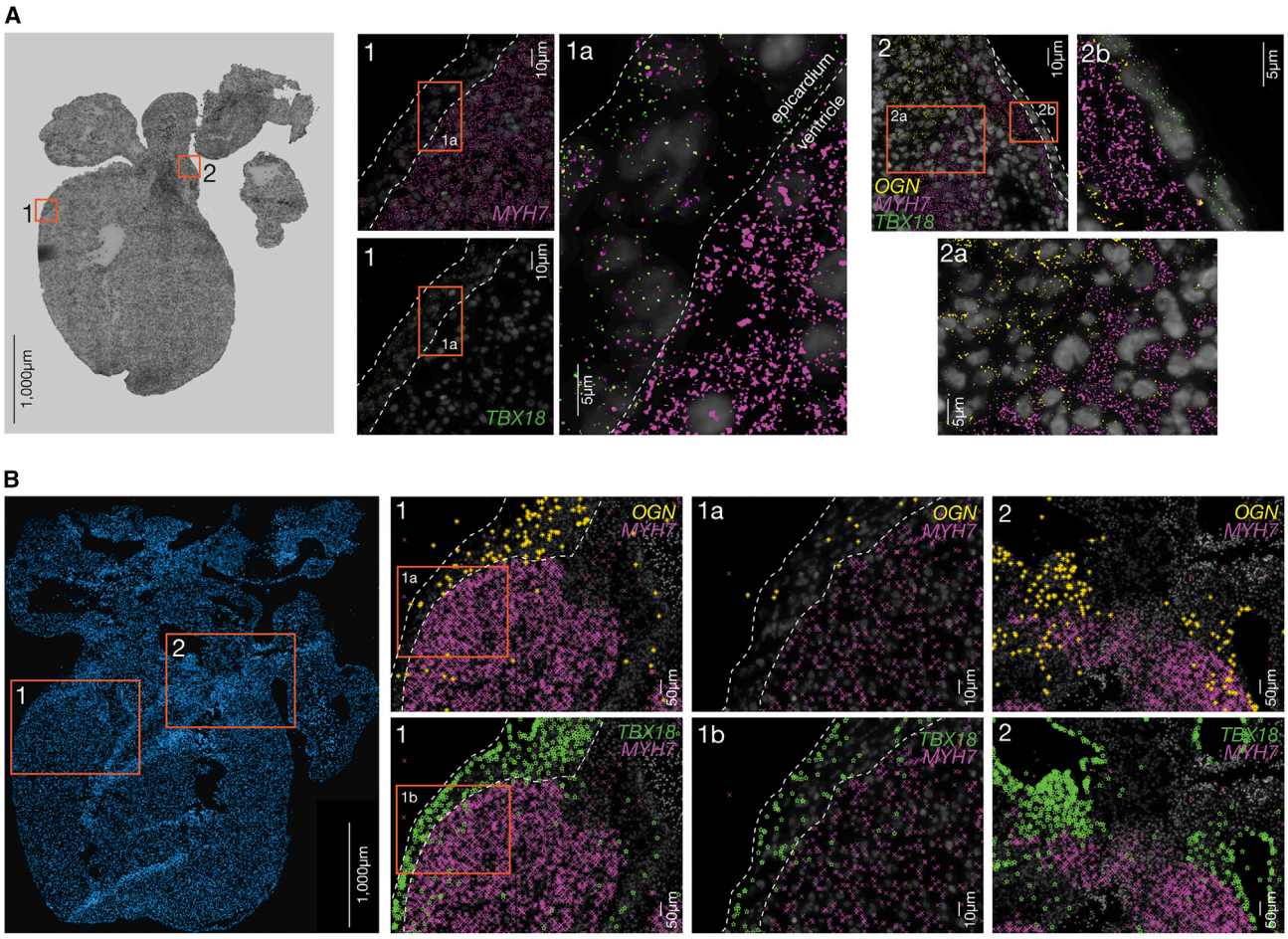

Figure 4. Validation of ISS Data by smFISH

(A) A tissue section from the 6.5 PCW heart sample analyzed by smFISH and showing spatial distribution of the *MYH7*, *TBX18*, and *OGN* genes. Scale bars: (A) 1,000 μm, (A1) 10 μm, (A1a) 5 μm, (A2) 10 μm, and (A2a-b) 5 μm.

(B) A tissue section from the 6.5 PCW heart sample analyzed by ISS, demonstrating matching gene expression patterns. *MYH7* was localized in the ventricles, *TBX18* was localized in the epicardium, and *OGN* was localized toward the OFT region. Scale bars: (B) 1,000 μm, (B1) 50 μm, (B1a-b) 10 μm, and (B2) 50 μm.

(A and B) Figures contain tiled images to cover the entire tissue.

stages, we discovered that cardiac neural crest cells were present only in the earlier stages, while Schwann progenitor cells were only seen in the later stages (Figures 6C and 6D). Moreover, cardiac neural crest cells were not present in the AV sub-epicardial mesenchyme at any time point, but the Schwann progenitor cells populated this domain during the later stages (Figures 6E and 6F).

We also defined the major differences between epicardial cells (cluster 9) and EPDCs (cluster 3). Epicardial cells were characterized by the expression of *ITLN1,* which was found in the epicardial layer surrounding the heart. The marker gene *TBX18* was expressed by both cell types (Wu et al., 2013), while *TCF21* (Braitsch and Yutzey, 2013) was more localized in the sub-epicardium, where EPDCs are found (Figure 6B). The temporal analysis presented in Figures 6E and 6F shows the localization of the epicardial cells (*ITLN1*, *TBX18*) and EPDCs (*TBX18*) within the AV sub-epicardial mesenchyme at all three time points. In the 4.5–5 PCW heart, the epicardium barely covered the pericardial surface of the heart, and only traces of developing sub-epicardium were detectable. Conversely, at the two later time points, the AV sub-epicardial mesenchyme had been formed and populated by EPDCs. Similar results were obtained with the other technical replicates (Figures S5B–S5E).

We also dissected the scRNA-seq cluster conglomerate (Figure 3B) consisting of EPDCs (cluster 3) and fibroblast-like cells (clusters 2, 4, 5, and 8). A deeper examination of these clusters revealed that they possessed distinct spatial locations coupled to unique functional properties (Figures S5A and S6). EPDCs were mostly present in the AV sub-epicardial mesenchyme (Figure 6G) and were primarily involved in organ and muscle development (Figure S6B). Among the fibroblast-like cells, those associated with cluster 2 were mainly located at the base of the OFT and in the valve apparatus, while cluster 5 was mainly localized within the OFT and was involved in its morphogenesis. Cluster 5 was also represented in the AV sub-epicardial mesenchyme, suggesting some involvement in

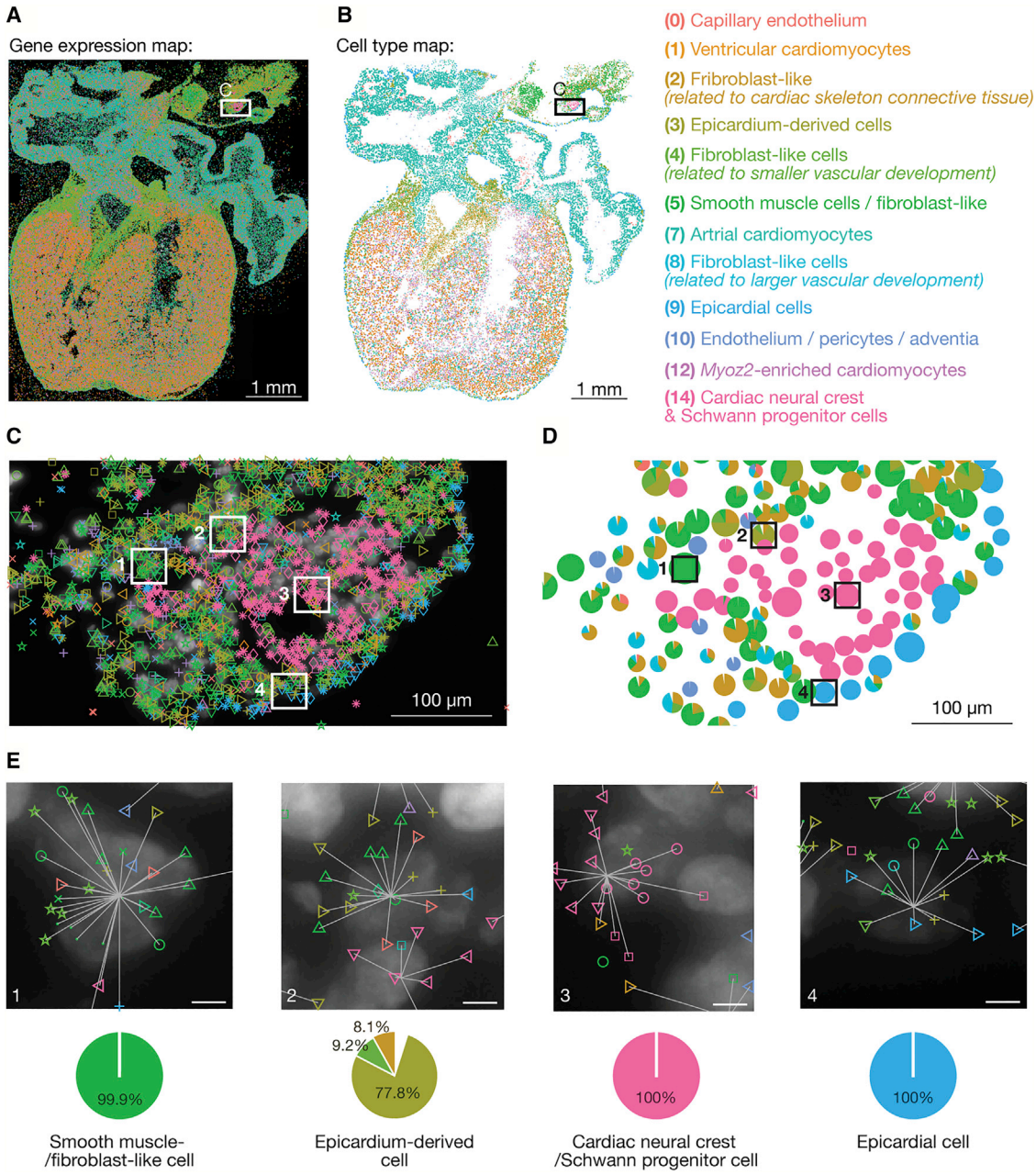

Figure 5. Cell-Type Map of the Human Developing Heart at the Intermediate Stage

(A) Distribution of the 69 gene transcripts identified by ISS in a 6.5 PCW heart tissue section. Gene signals are displayed as symbols with colors grouped according to their cluster belonging as seen in Figure 3B. Only reads assigned to cells were included for further analysis. The region in the white square is magnified in (C). Scale bar, 1 mm.

(B) Probabilistic cell map of the gene transcripts shown in (A). The map displays 20,920 cells represented as pie charts of probabilities matching the scRNA-seq clusters. Each pie proportion is color coded as in Figure 3B. The region in the black square is magnified in (D). Scale bar, 1 mm.

(C) Magnified image of the selected area in (A). Identified gene signals are shown as colored symbols based on their cluster identity. White squares are zoomed-in single cells in (E). Scale bar, 100 µm.

(D) Magnified image of corresponding area in (B). Each pie chart represents a single cell and its size is proportional to the number of reads (minimum 5) assigned to the cell. Black squares are zoomed-in single cells illustrated in (E). Scale bar, 100 µm.

(E) Distribution and assignment of reads, and probability distributions of cell clusters at single-cell level. Examples from (C) and (D) show how reads are assigned to cells and how cells are assigned to cluster. Top panel: distribution and assignment of reads to four example cells. White lines join reads to the cell that they are assigned to. Cell nuclei stained with DAPI are shown in gray. Bottom panel: pie charts showing how cells match to each cluster for the above mentioned four example cells. Colors are cell-type specific. Scale bars, 5 µm.

(A) Figure contains tiled images to cover the entire tissue.

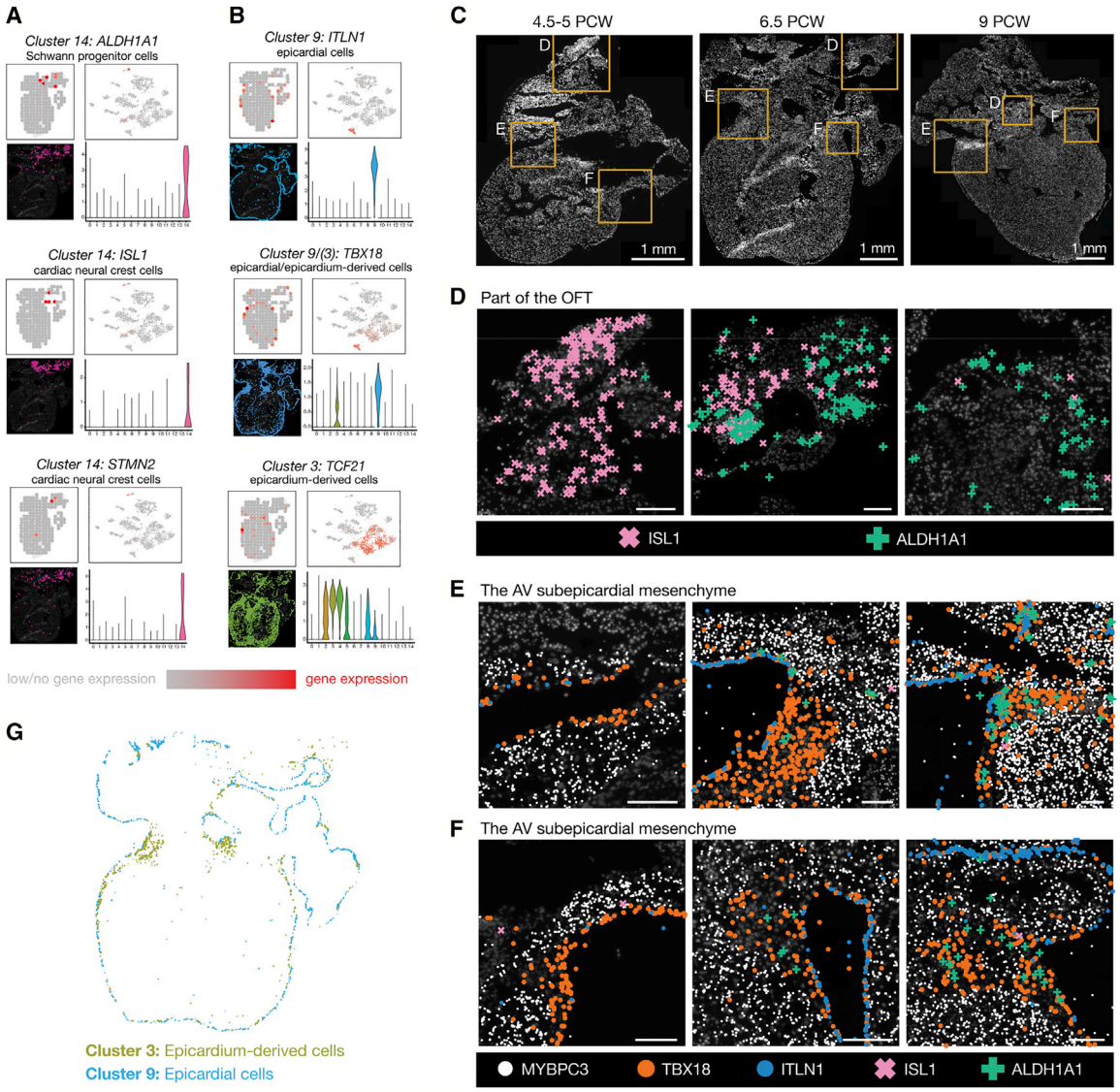

Figure 6. Targeted Spatiotemporal Analysis on the Three Cardiac Developmental Stages

(A and B) Comparison of gene expression detection across ST, scRNA-seq, and ISS for marker genes specific for Schwann progenitor and cardiac neural crest cells (A) and epicardial cells and EPDCs (B). Each marker gene expression is illustrated as heatmap in ST tissue sections and scRNA-seq tSNE plot, as violin plot throughout the scRNA-seq clusters and as registered transcripts in ISS tissue sections, respectively.

(C) Overview of three cardiac tissue sections at 4.5–5, 6.5, and 9 PCW, respectively. Yellow squares indicate tissue domains that are magnified and showed in (D–F). Scale bars, 1 mm.

(D) Magnified images of the OFT domain in the three time points showing subcellular gene expressions of *ISL1* and *ALDH1A1* detected by ISS. Scale bar, 200 μm.

(E and F) Magnified images of the right (E) and left (F) AV subepicardial mesenchyme domain in the three time points showing subcellular gene expressions of *MYBPC3*, *TBX18*, *ITLN1*, *ISL1*, and *ALDH1A1* detected by ISS. Scale bar, 200 μm.

(G) Spatial distribution of epicardial cells (cluster 9) and EPDCs (cluster 3) based on the probabilistic cell mapping. Each data point (i.e., cell) is represented by a pie chart color coded as in Figure 3B.

(A–F) Figures contain tiled images to cover the entire tissue.

coronary artery formation (Figure S6). Clusters 4 and 8 had similar spatial patterns. However, cluster 4 was more evident in the sub-epicardium and involved in connective tissue development and vasculogenesis, while cluster 8 was localized slightly more towards the OFT and related more specifically to artery and aorta morphogenesis and regulation of endothelial cell proliferation.

Importantly, we found three types of cardiomyocytes (Figure 3B), which were detected at all three investigated developmental stages. Two of them expressed markers specific for atrial and ventricular cardiomyocytes in agreement with their spatial localization (Figure S5A). Instead, the third population, expressing *MYOZ2* and *FABP3*, was localized both in the atria and ventricles but had not been previously described in human

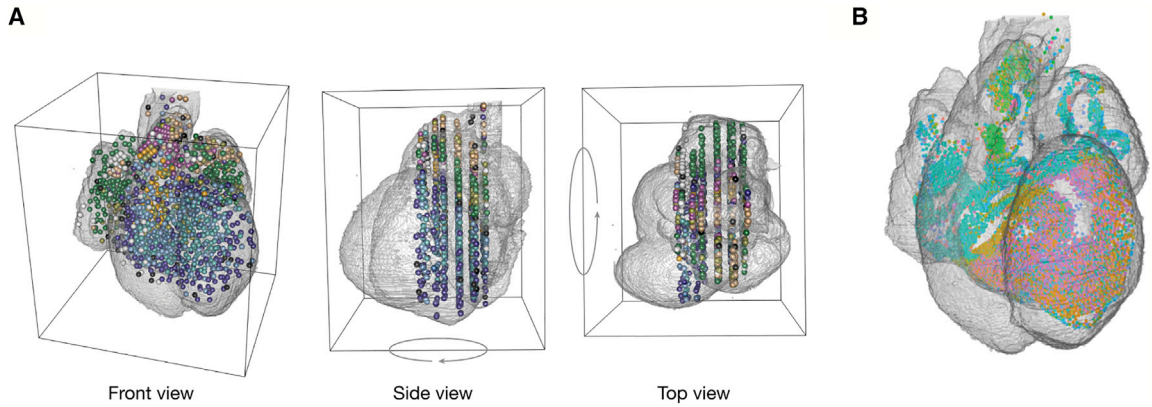

Figure 7. A 3D Gene Expression Atlas

(A) A digital construction of a 3D gene expression reference model of the 6.5 PCW human embryonic heart. The model illustrates here the locations of ST spots from the nine ST tissue sections viewed from the front, side, and top. ST spots are colored by their cluster identity seen in Figure 2F.

(B) The same 3D digital construction as seen in (A), but here illustrating the ISS probabilistic cell map. The image displays all 20,920 cells from one 6.5 PCW tissue section, colored by their cell type identity as in Figure 3B.

heart development. We named this new population of cardiomyocytes *Myoz2*-enriched cardiomyocytes because it was recently described in the adult mouse heart (Gladka et al., 2018).

Finally, a closer spatial examination of the two endothelial cell types (clusters 0 and 10) showed that the former type (annotated as capillary endothelium) was mainly localized in the trabecular myocardium, where blood is mainly supplied via smaller vessels (primarily capillaries). Conversely, the latter type (annotated as endothelium/pericytes/adventia) was mainly localized in the compact myocardium, where coronary arteries supply the heart with oxygenated blood (Figures S5B–S5E). Collectively, these findings demonstrate the key role of spatial gene expression analysis in distinguishing the localization and function of relatively similar cell types.

To facilitate the use of our atlas, we provide a publicly available web resource to visually explore spatial gene expression patterns that regulate human cardiac development (https://hdca-sweden.scilifelab.se/a-study-on-human-heart-development/). This resource contains an explorer for ST and scRNA-seq data, a viewer of ISS information, and a 3D viewer of the 6.5 PCW embryonic heart. The nine ST tissue sections building up the 3D model can be interrogated for global and single spatial gene expression patterns in order to investigate both general and detailed dynamics of cardiac organogenesis (Figure 7A). In addition, the spatial cell map derived from ISS data was aligned to the 3D model to provide cellular resolution (Figure 7B).

DISCUSSION

Understanding the biological functions, networks, and interactions of the different cell types that regulate organ and disease development requires both cellular information and a spatial context. Various pioneering approaches that combine spatial information with scRNA-seq data have been reported (Moncada et al., 2019; Achim et al., 2015; Satija et al., 2015; Karaiskos et al., 2017). However, most of them are computational strategies for studying the development of model organisms by exploiting pre-existing *in situ* hybridization landmark gene data (Achim et al., 2015; Satija et al., 2015; Karaiskos et al., 2017). Because model systems cannot reflect subtle differences between species, detailed information of this sort cannot be readily applied in studies on human organogenesis. Consequently, there is a clear need for spatially resolved single-cell transcriptional data on human developmental tissues.

Here, we present an innovative approach that combines the power of three different technologies (ST, scRNA-seq, and ISS) to comprehensively characterize spatial and temporal differences in gene expression during human cardiac morphogenesis at an organ-wide level with single-cell resolution. We obtained transcriptional snapshots from four human embryonic hearts spanning three different developmental stages (4.5–5, 6.5–7, and 9 PCW), enabling analysis of the progression of cardiac structure formation. While it would be very interesting to study formative processes in earlier human cardiac tissues, doing so would present substantial practical difficulties.

Each of these technologies has key features that allowed us to generate a well-resolved cellular map of the developing human heart. We used the exploratory power of ST to identify spatial genome-wide expression patterns common to the three developmental stages. Additionally, cell-type heterogeneity in the intermediate developmental stage was deconvolved using scRNA-seq. The combination of these two technologies allowed us to identify a comprehensive set of gene probes that could summarize the spatial and cellular information, recreating the overall complexity of the developing human heart. Finally, the targeted resolution of ISS enabled us to create a refined subcellular gene expression map across the three developmental stages. In this way, we established a molecular approach for studying the spatiotemporal gene expression patterns of the developing human heart at the cellular level.

Our concerted use of these techniques revealed that global spatial gene expression patterns are established early (4.5–5 PCW) in embryonic heart development and are maintained

up until 9 PCW. In particular, we observed conserved spatial gene expression patterns in the ventricular and atrial myocardium, AV mesenchyme, epicardium, and OFT regions. In contrast, there are spatiotemporal differences in the association between the epicardium, EPDC formation, and the formation of fibroblasts, vascular structures, the annulus fibrosus, and the valvular and muscular structures during the three developmental stages. Specifically, epicardial spatial marker genes identified by ST were expressed by the two cell types annotated as epicardial cells and EPDCs in the single-cell analysis. The inclusion of these genes in our ISS gene panel revealed that whereas the surface of the 4.5–5 PCW heart was covered by epicardial cells, EPDC formation via epithelial-to-mesenchymal transition had only just begun at this developmental stage. At the later developmental stages, EPDC formation had continued in the AV subepicardial mesenchyme and is likely to have subsequently contributed to the differentiation of several fibroblast-like cell types. It is not yet clear whether the EPDCs can also differentiate into cardiomyocytes or influence cardiomyocyte differentiation via exosomes.

Another notable finding is that cardiac neural crest cells and Schwann progenitor cells exhibit distinct spatiotemporal patterns. Specifically, cardiac neural crest cells are uniquely present in the mediastinum and OFT in early stages of cardiac development. This corroborates the analysis of Keyte et al. (2014), who suggested that cardiac neural crest cells are required for the septation of the OFT into its aortic and pulmonary components during the developmental stages analyzed here. Conversely, Schwann progenitor cells appear in the mediastinum and the OFT first in the later developmental stages. In addition, their presence within the AV sub-epicardial mesenchyme region is also only seen in the later developmental stages. The exact relationship between cardiac neural crest cells and Schwann progenitor cells is yet not finally resolved.

Our approach also allowed us to identify differences within the scRNA-seq cluster conglomerate populated by the EPDCs and four different fibroblast-like cell types and between two endothelial cell types. The cluster conglomerate was observed in earlier studies (DeLaughter et al., 2016; Gladka et al., 2018; Cui et al., 2019) but has not previously been dissected. We found that each of the four fibroblast-like cell types and the two endothelial cell types have specific spatial locations and serve distinct functions during cardiac development. Additionally, we showed that one of the unique fibroblast-like cell types (fibroblast-like/smooth muscle cells, scRNA-seq cluster 5), together with endothelial cells, contributes to the formation of coronary arteries in the developing heart.

Finally, we identified three types of cardiomyocytes. Two of them, atrial and ventricular cardiomyocytes, were specifically localized in the atria and ventricles, respectively, while the third one, *Myoz2*-enriched cardiomyocytes, was present in both anatomical domains. Importantly, this population had an expression profile similar to the one that has been recently described in the adult mouse heart (Gladka et al., 2018) but had not been previously described in human heart development. Exploring the biological function of this subset of cardiomyocytes could give important information into mechanisms responsible for heart function and cardiac pathologies, given the documented role of *MYOZ2* in a subset of hypertrophic cardiomyopathy (Osio et al., 2007).

In conclusion, we have studied human heart development using a single-cell spatiotemporal approach and constructed a molecular approach that could be used to explore developmental processes in other organisms where little information is available. Our approach makes it possible to explore global spatial transcriptional patterns in tissues, deconvolve their cellular heterogeneity, and selectively target key genes with spatially heterogeneous expression patterns that are responsible for cell-type differences. Our model of the developing human heart is, to our knowledge, one of the first organ-wide human developmental-transcriptional atlases with single-cell spatial resolution. To facilitate its exploitation, we have created a publicly available web resource that can be used to investigate and visualize 2D and 3D models (https://hdca-sweden.scilifelab.se/a-study-on-human-heart-development/) of spatiotemporal gene expression patterns during heart development. These models clearly show that the integration of spatial and temporal information with single-cell gene expression data is essential for the identification of key differences between cell types and detailed analysis of developing tissues.

STAR★METHODS

Detailed methods are provided in the online version of this paper and include the following:

- KEY RESOURCES TABLE
- LEAD CONTACT AND MATERIALS AVAILABILITY
- EXPERIMENTAL MODEL AND SUBJECT DETAILS
  - Human developmental tissue
- METHOD DETAILS
  - Experimental design
  - Quality control arrays and spatially barcoded arrays
  - Preparation of human developing hearts
  - Hematoxylin & eosin staining and imaging
  - Immunohistochemistry
  - Specific optimizations of the ST protocol for developmental heart tissue
  - Library preparations and sequencing
  - Image alignment of ST tissue and spots
  - Rolling circle amplification (RCA) and *in situ* sequencing (ISS)
  - Single-molecule fluorescent *in situ* hybridization (smFISH)
- QUANTIFICATION AND STATISTICAL ANALYSIS
  - Sequence alignment and annotation
  - Data quality and filtering
  - Data processing
  - Cluster visualization and differential gene expression analysis
  - Gene ontology enrichment of gene clusters
  - Bulk treated ST and single-cell data
  - ISS image analysis, decoding and single cell analysis
  - Probabilistic spatial cell map based on ISS data
  - Constructing a reference atlas of a human embryonic heart

SUPPLEMENTAL INFORMATION

Supplemental Information can be found online at https://doi.org/10.1016/j.cell.2019.11.025.

ACKNOWLEDGMENTS

We thank Annelie Mollbrink, PhD, and Erik Wernersson, PhD, for help with experiments. We also thank Matthias Corbascio and Karl-Henrik Grinnemo for discussions and Phil Ewels for critically reviewing the manuscript. We thank the Swedish National Genomics Infrastructure (NGI) and the Eukaryotic Single Cell Genomics facility (ESCG), hosted at SciLifeLab, for infrastructure support. We thank the National Bioinformatics Infrastructure Sweden (NBIS) for computational assistance and Uppsala Multidisciplinary Center for Advanced Computational Science (UPPMAX) for providing computational infrastructure. We thank the KI Developmental Tissue Bank for providing tissue material. We also thank the Live Cell Imaging Facility, Karolinska Institutet (KI), Sweden, with core facility support from the KI infrastructure committee and the Centre for Innovative Medicine at KI. This work was supported by the Erling-Persson family foundation, the Knut and Alice Wallenberg Foundation, the Swedish Research Council, the Jonasson Center at the Royal Institute of Technology (Sweden) and StratRegen at KI. S.G. and J.R. were financially supported by the Knut and Wallenberg Foundation as part of the National Bioinformatics Infrastructure Sweden at SciLifeLab. S.G. was also supported by Formas grant 2017-01066_3.

AUTHOR CONTRIBUTIONS

M.A. designed the study, planned and performed the experiments, analyzed the data, interpreted results, wrote the manuscript, and designed and prepared figures. S.G. guided data analysis, analyzed the data, interpreted results, wrote the manuscript, and designed figures. L.L. analyzed the data and interpreted results that contributed to the final manuscript. C.W. performed *in situ* sequencing experiments and analyzed ISS data. D.F. constructed the 3D reference atlas of the human embryonic heart. X.Q. performed spatial cell type mapping of ISS data and prepared figures and ISS online viewer. E.W. performed tissue sectioning, immunohistochemical staining, guided histological annotations, and prepared and dissociated heart tissue to a single-cell solution. J.C. performed smFISH experiments. J.R. assisted in data analysis. F.S. assisted in experimental set-up and data analysis. C.Ö. assisted in the set-up of embryonic material. E.S. and E.Å. dissected and staged the tissue material. M.B. guided smFISH experiments. A.M.-B. assisted in biological guidance. P.L.S. assisted in experimental set-up and data analysis. M.N. guided *in situ* sequencing experiments. C.S. provided biological guidance, analyzed the data, interpreted biological results, and wrote the manuscript. J.L. conceived and designed the study. All authors helped with manuscript preparation.

DECLARATION OF INTERESTS

S.G., P.L.S., and J.L. are scientific advisors to 10x Genomics, which holds IP rights to the ST technology. M.N. and X.Q. hold shares in Cartana AB, a company commercializing *in situ* sequencing reagents.

Received: June 28, 2018
Revised: September 6, 2019
Accepted: November 14, 2019
Published: December 12, 2019

REFERENCES

Achim, K., Pettit, J.B., Saraiva, L.R., Gavriouchkina, D., Larsson, T., Arendt, D., and Marioni, J.C. (2015). High-throughput spatial mapping of single-cell RNA-seq data to tissue of origin. Nat. Biotechnol. *33*, 503–509.

Anders, S., Pyl, P.T., and Huber, W. (2015). HTSeq–a Python framework to work with high-throughput sequencing data. Bioinformatics *31*, 166–169.

Anderson, D.J., and Axel, R. (1985). Molecular probes for the development and plasticity of neural crest derivatives. Cell *42*, 649–662.

Asp, M., Salmén, F., Ståhl, P.L., Vickovic, S., Felldin, U., Löfling, M., Fernandez Navarro, J., Maaskola, J., Eriksson, M.J., Persson, B., et al. (2017). Spatial detection of fetal marker genes expressed at low level in adult human heart tissue. Sci. Rep. *7*, 12941.

Bookstein, F.L. (1989). Principal warps: thin-plate splines and the decomposition of deformations. IEEE Trans. Pattern Anal. Mach. Intell. *11*, 567–585.

Braitsch, C.M., and Yutzey, K.E. (2013). Transcriptional Control of Cell Lineage Development in Epicardium-Derived Cells. J. Dev. Biol. *1*, 92–111.

Burzynski, G.M., Delalande, J.-M., and Shepherd, I. (2009). Characterization of spatial and temporal expression pattern of SCG10 during zebrafish development. Gene Expr. Patterns *9*, 231–237.

Cai, C.L., Martin, J.C., Sun, Y., Cui, L., Wang, L., Ouyang, K., Yang, L., Bu, L., Liang, X., Zhang, X., et al. (2008). A myocardial lineage derives from Tbx18 epicardial cells. Nature *454*, 104–108.

Chen, K.H., Boettiger, A.N., Moffitt, J.R., Wang, S., and Zhuang, X. (2015). RNA imaging. Spatially resolved, highly multiplexed RNA profiling in single cells. Science *348*, aaa6090.

Costea, P.I., Lundeberg, J., and Akan, P. (2013). TagGD: fast and accurate software for DNA Tag generation and demultiplexing. PLoS ONE *8*, e57521.

Cui, Y., Zheng, Y., Liu, X., Yan, L., Fan, X., Yong, J., Hu, Y., Dong, J., Li, Q., Wu, X., et al. (2019). Single-Cell Transcriptome Analysis Maps the Developmental Track of the Human Heart. Cell Rep. *26*, 1934–1950.e5.

de Bakker, B.S., de Jong, K.H., Hagoort, J., de Bree, K., Besselink, C.T., de Kanter, F.E., Veldhuis, T., Bais, B., Schildmeijer, R., Ruijter, J.M., et al. (2016). An interactive three-dimensional digital atlas and quantitative database of human development. Science *354*, aag0053.

DeLaughter, D.M., Bick, A.G., Wakimoto, H., McKean, D., Gorham, J.M., Kathiriya, I.S., Hinson, J.T., Homsy, J., Gray, J., Pu, W., et al. (2016). Single-Cell Resolution of Temporal Gene Expression during Heart Development. Dev. Cell *39*, 480–490.

Dobin, A., Davis, C.A., Schlesinger, F., Drenkow, J., Zaleski, C., Jha, S., Batut, P., Chaisson, M., and Gingeras, T.R. (2013). STAR: ultrafast universal RNA-seq aligner. Bioinformatics *29*, 15–21.

Eng, C.L., Lawson, M., Zhu, Q., Dries, R., Koulena, N., Takei, Y., Yun, J., Cronin, C., Karp, C., Yuan, G.C., and Cai, L. (2019). Transcriptome-scale super-resolved imaging in tissues by RNA seqFISH. Nature *568*, 235–239.

Engleka, K.A., Manderfield, L.J., Brust, R.D., Li, L., Cohen, A., Dymecki, S.M., and Epstein, J.A. (2012). Islet1 derivatives in the heart are of both neural crest and second heart field origin. Circ. Res. *110*, 922–926.

Fürth, D., Vaissière, T., Tzortzi, O., Xuan, Y., Märtin, A., Lazaridis, I., Spigolon, G., Fisone, G., Tomer, R., Deisseroth, K., et al. (2018). An interactive framework for whole-brain maps at cellular resolution. Nat. Neurosci. *21*, 139–149.

Gelali, E., Custodio, J., Girelli, G., Wernersson, E., Crosetto, N., and Bienko, M. (2018). An Application-Directed, Versatile DNA FISH Platform for Research and Diagnostics. Methods Mol. Biol. *1766*, 303–333.

Gelali, E., Girelli, G., Matsumoto, M., Wernersson, E., Custodio, J., Mota, A., Schweitzer, M., Ferenc, K., Li, X., Mirzazadeh, R., et al. (2019). iFISH is a publically available resource enabling versatile DNA FISH to study genome architecture. Nat. Commun. *10*, 1636.

Giacomello, S., and Lundeberg, J. (2018). Preparation of plant tissue to enable Spatial Transcriptomics profiling using barcoded microarrays. Nat. Protoc. *13*, 2425–2446.

Giacomello, S., Salmén, F., Terebieniec, B.K., Vickovic, S., Navarro, J.F., Alexeyenko, A., Reimegård, J., McKee, L.S., Mannapperuma, C., Bulone, V., et al. (2017). Spatially resolved transcriptome profiling in model plant species. Nat. Plants *3*, 17061.

Gladka, M.M., Molenaar, B., de Ruiter, H., van der Elst, S., Tsui, H., Versteeg, D., Lacraz, G.P.A., Huibers, M.M.H., van Oudenaarden, A., and van Rooij, E. (2018). Single-Cell Sequencing of the Healthy and Diseased Heart Reveals Cytoskeleton-Associated Protein 4 as a New Modulator of Fibroblasts Activation. Circulation *137*, 166–180.

Groves, A.K., George, K.M., Tissier-Seta, J.P., Engel, J.D., Brunet, J.F., and Anderson, D.J. (1995). Differential regulation of transcription factor gene expression and phenotypic markers in developing sympathetic neurons. Development *121*, 887–901.

Jemt, A., Salmén, F., Lundmark, A., Mollbrink, A., Fernández Navarro, J., Ståhl, P.L., Yucel-Lindberg, T., and Lundeberg, J. (2016). An automated approach to prepare tissue-derived spatially barcoded RNA-sequencing libraries. Sci. Rep. *6*, 37137.

Jessen, K.R., and Mirsky, R. (2019). Schwann Cell Precursors; Multipotent Glial Cells in Embryonic Nerves. Front. Mol. Neurosci. *12*, 69.

Junker, J.P., Noël, E.S., Guryev, V., Peterson, K.A., Shah, G., Huisken, J., McMahon, A.P., Berezikov, E., Bakkers, J., and van Oudenaarden, A. (2014). Genome-wide RNA Tomography in the zebrafish embryo. Cell *159*, 662–675.

Karaiskos, N., Wahle, P., Alles, J., Boltengagen, A., Ayoub, S., Kipar, C., Kocks, C., Rajewsky, N., and Zinzen, R.P. (2017). The *Drosophila* embryo at single-cell transcriptome resolution. Science *358*, 194–199.

Ke, R., Mignardi, M., Pacureanu, A., Svedlund, J., Botling, J., Wählby, C., and Nilsson, M. (2013). In situ sequencing for RNA analysis in preserved tissue and cells. Nat. Methods *10*, 857–860.

Keyte, A.L., Alonzo-Johnsen, M., and Hutson, M.R. (2014). Evolutionary and developmental origins of the cardiac neural crest: building a divided outflow tract. Birth Defects Res. C Embryo Today *102*, 309–323.

Kowalczyk, M.S., Tirosh, I., Heckl, D., Rao, T.N., Dixit, A., Haas, B.J., Schneider, R.K., Wagers, A.J., Ebert, B.L., and Regev, A. (2015). Single-cell RNA-seq reveals changes in cell cycle and differentiation programs upon aging of hematopoietic stem cells. Genome Res. *25*, 1860–1872.

Lee, J.H., Daugharthy, E.R., Scheiman, J., Kalhor, R., Yang, J.L., Ferrante, T.C., Terry, R., Jeanty, S.S., Li, C., Amamoto, R., et al. (2014). Highly multiplexed subcellular RNA sequencing in situ. Science *343*, 1360–1363.

Lescroart, F., Wang, X., Lin, X., Swedlund, B., Gargouri, S., Sànchez-Dànes, A., Moignard, V., Dubois, C., Paulissen, C., Kinston, S., et al. (2018). Defining the earliest step of cardiovascular lineage segregation by single-cell RNA-seq. Science *359*, 1177–1181.

Li, G., Xu, A., Sim, S., Priest, J.R., Tian, X., Khan, T., Quertermous, T., Zhou, B., Tsao, P.S., Quake, S.R., and Wu, S.M. (2016). Transcriptomic profiling maps anatomically patterned subpopulations among single embryonic cardiac cells. Dev. Cell *39*, 491–507.

Lin, L., Sylvén, C., Sotonyi, P., Somogyi, E., Kaijser, L., and Jansson, E. (1990). Myoglobin content and citrate synthase activity in different parts of the normal human heart. J. Appl. Physiol. *69*, 899–901.

Lovatt, D., Ruble, B.K., Lee, J., Dueck, H., Kim, T.K., Fisher, S., Francis, C., Spaethling, J.M., Wolf, J.A., Grady, M.S., et al. (2014). Transcriptome in vivo analysis (TIVA) of spatially defined single cells in live tissue. Nat. Methods *11*, 190–196.

Lundmark, A., Gerasimcik, N., Båge, T., Jemt, A., Mollbrink, A., Salmén, F., Lundeberg, J., and Yucel-Lindberg, T. (2018). Gene expression profiling of periodontitis-affected gingival tissue by spatial transcriptomics. Sci. Rep. *8*, 9370.

Maniatis, S., Äijö, T., Vickovic, S., Braine, C., Kang, K., Mollbrink, A., Fagegaltier, D., Andrusivová, Ž., Saarenpää, S., Saiz-Castro, G., et al. (2019). Spatiotemporal dynamics of molecular pathology in amyotrophic lateral sclerosis. Science *364*, 89–93.

Månsson-Broberg, A., Rodin, S., Bulatovic, I., Ibarra, C., Löfling, M., Genead, R., Wärdell, E., Felldin, U., Granath, C., Alici, E., et al. (2016). Wnt/β-Catenin Stimulation and Laminins Support Cardiovascular Cell Progenitor Expansion from Human Fetal Cardiac Mesenchymal Stromal Cells. Stem Cell Reports *6*, 607–617.

Masters, M., and Riley, P.R. (2014). The epicardium signals the way towards heart regeneration. Stem Cell Res. (Amst.) *13* (3 Pt B), 683–692.

McGinnis, C.S., Murrow, L.M., and Gartner, Z.J. (2019). DoubletFinder: Doublet Detection in Single-Cell RNA Sequencing Data Using Artificial Nearest Neighbors. Cell Syst. *8*, 329–337.e4.

Meilhac, S.M., and Buckingham, M.E. (2018). The deployment of cell lineages that form the mammalian heart. Nat. Rev. Cardiol. *15*, 705–724.

Moffitt, J.R., and Zhuang, X. (2016). RNA Imaging with Multiplexed Error-Robust Fluorescence In Situ Hybridization (MERFISH). Methods Enzymol. *572*, 1–49.

Moncada, R., Wagner, F., Chiodin, M., Devlin, J.C., Baron, M., Hajdu, C.H., Simeone, D.M., and Yanai, I. (2019). Integrating single-cell RNA-Seq with spatial transcriptomics in pancreatic ductal adenocarcinoma using multimodal intersection analysis. bioRxiv. https://doi.org/10.1101/254375.

Moss, J.B., Xavier-Neto, J., Shapiro, M.D., Nayeem, S.M., McCaffery, P., Dräger, U.C., and Rosenthal, N. (1998). Dynamic patterns of retinoic acid synthesis and response in the developing mammalian heart. Dev. Biol. *199*, 55–71.

Navarro, J.F., Sjöstrand, J., Salmén, F., Lundeberg, J., and Ståhl, P.L. (2017). ST Pipeline: an automated pipeline for spatial mapping of unique transcripts. Bioinformatics *33*, 2591–2593.

Osio, A., Tan, L., Chen, S.N., Lombardi, R., Nagueh, S.F., Shete, S., Roberts, R., Willerson, J.T., and Marian, A.J. (2007). Myozenin 2 is a novel gene for human hypertrophic cardiomyopathy. Circ. Res. *100*, 766–768.

Petersen, J., and Adameyko, I. (2017). Nerve-associated neural crest: peripheral glial cells generate multiple fates in the body. Curr. Opin. Genet. Dev. *45*, 10–14.

Qian, X., Harris, K.D., Hauling, T., Nicoloutsopoulos, D., Muñoz-Manchado, A.B., Skene, N., Hjerling-Leffler, J., and Nilsson, M. (2019). Probabilistic cell typing enables fine mapping of closely related cell types in situ. Nat. Methods. Published online November 18, 2019. https://doi.org/10.1038/s41592-019-0631-4.

Ray, P.F., Winston, R.M.L., and Handyside, A.H. (1997). XIST expression from the maternal X chromosome in human male preimplantation embryos at the blastocyst stage. Hum. Mol. Genet. *6*, 1323–1327.

Regev, A., Teichmann, S.A., Lander, E.S., Amit, I., Benoist, C., Birney, E., Bodenmiller, B., Campbell, P., Carninci, P., Clatworthy, M., et al.; Human Cell Atlas Meeting Participants (2017). The Human Cell Atlas. Elife *6*, e27041.

Rodriques, S.G., Stickels, R.R., Goeva, A., Martin, C.A., Murray, E., Vanderburg, C.R., Welch, J., Chen, L.M., Chen, F., and Macosko, E.Z. (2019). Slide-seq: A scalable technology for measuring genome-wide expression at high spatial resolution. Science *363*, 1463–1467.

Sahara, M., Santoro, F., Sohlmér, J., Zhou, C., Witman, N., Leung, C.Y., Mononen, M., Bylund, K., Gruber, P., and Chien, K.R. (2019). Population and Single-Cell Analysis of Human Cardiogenesis Reveals Unique LGR5 Ventricular Progenitors in Embryonic Outflow Tract. Dev. Cell *48*, 475–490.e7.

Salmén, F., Ståhl, P.L., Mollbrink, A., Navarro, J.F., Vickovic, S., Frisén, J., and Lundeberg, J. (2018). Barcoded solid-phase RNA capture for Spatial Transcriptomics profiling in mammalian tissue sections. Nat. Protoc. *13*, 2501–2534.

Satija, R., Farrell, J.A., Gennert, D., Schier, A.F., and Regev, A. (2015). Spatial reconstruction of single-cell gene expression data. Nat. Biotechnol. *33*, 495–502.

Ståhl, P.L., Salmén, F., Vickovic, S., Lundmark, A., Navarro, J.F., Magnusson, J., Giacomello, S., Asp, M., Westholm, J.O., Huss, M., et al. (2016). Visualization and analysis of gene expression in tissue sections by spatial transcriptomics. Science *353*, 78–82.

Sylva, M., van den Hoff, M.J., and Moorman, A.F. (2014). Development of the human heart. Am. J. Med. Genet. A. *164A*, 1347–1371.

Vickovic, S., Eraslan, G., Salmén, F., Klughammer, J., Stenbeck, L., Schapiro, D., Äijö, T., Bonneau, R., Bergenstråhle, L., Navarro, J.F., et al. (2019). High-definition spatial transcriptomics for in situ tissue profiling. Nat. Methods *16*, 987–990.

Wang, X., Allen, W.E., Wright, M.A., Sylwestrak, E.L., Samusik, N., Vesuna, S., Evans, K., Liu, C., Ramakrishnan, C., Liu, J., and Nolan, G.P. (2018). Three-dimensional intact-tissue sequencing of single-cell transcriptional states. Science *361*, eaat5691.

Wu, S.P., Dong, X.R., Regan, J.N., Su, C., and Majesky, M.W. (2013). Tbx18 regulates development of the epicardium and coronary vessels. Dev. Biol. *383*, 307–320.

Yu, G., Wang, L.G., Han, Y., and He, Q.Y. (2012). clusterProfiler: an R package for comparing biological themes among gene clusters. OMICS *16*, 284–287.

Zheng, G.X., Terry, J.M., Belgrader, P., Ryvkin, P., Bent, Z.W., Wilson, R., Ziraldo, S.B., Wheeler, T.D., McDermott, G.P., Zhu, J., et al. (2017). Massively parallel digital transcriptional profiling of single cells. Nat. Commun. *8*, 14049.

STAR★METHODS

KEY RESOURCES TABLE

REAGENT or RESOURCE	SOURCE	IDENTIFIER
Antibodies		
Anti-Cardiac Troponin T antibody [1C11]	Abcam	ab8295
Monoclonal Anti-Actin, α-Smooth Muscle	Sigma Aldrich	A2547
Goat anti-Mouse IgG1 Cross-Adsorbed Secondary Antibody, Alexa Fluor 488	Thermo Fischer Scientific	A-21121
Goat anti-Mouse IgG2a Cross-Adsorbed Secondary Antibody, Alexa Fluor 568	Thermo Fischer Scientific	A-21134
Chemicals, Peptides, and Recombinant Proteins		
Trypsin (2.5%), no phenol red	Thermo Fischer Scientific	15090046
Collagenase, Type 2	Worthington Biochemical	LS004174
Pepsin	Sigma Aldrich	P7000-25G
Critical Commercial Assays		
Chromium Single Cell 3′ Library & Gel Bead Kit v2	10x Genomics	PN-120267
Deposited Data		
Raw sequence data	EBI-EGA	EGAS00001003996
Count matrixes	This paper	https://www.spatialresearch.org
High resolution ST images with cluster coordinates	Mendeley Data	https://dx.doi.org/10.17632/zkzvyprd5z.1
Raw image data	figshare	https://doi.org/10.6084/m9.figshare.10058048.v1
Web resource	This paper or Human Developmental Cell Atlas	https://hdca-sweden.scilifelab.se/a-study-on-human-heart-development/
Experimental Models: Organisms/Strains		
Human developmental heart tissue	Karolinska University Hospital	N/A
Oligonucleotides		
smFISH probes for: *OGN*	This paper	Table S4D
smFISH probes for: *MHY7*	This paper	Table S4D
smFISH probes for: *TBX18*	This paper	Table S4D
Software and Algorithms		
ST analysis pipeline v1.6.0	Navarro et al., 2017	https://github.com/SpatialTranscriptomicsResearch/st_pipeline
STAR v2.4.2a	Dobin et al., 2013	https://github.com/alexdobin/STAR/tree/STAR_2.4.2a
Cell Ranger Analysis Pipeline v2.1.1	10X Genomics	https://10xgenomics.com/
DoubletFinder v1.0.0	McGinnis et al., 2019	https://github.com/chris-mcginnis-ucsf/DoubletFinder
Seurat v2.3.4	Satija *et al.*, 2015	https://satijalab.org/seurat/install.html
MATLAB R2018a	MathWorks	https://mathworks.com/
MATLAB script to decode intensity information in situ sequencing data	Ke et al., 2013	https://github.com/Moldia/in_situ_seq
pciSeq	Qian et al., 2019	https://github.com/Moldia/heart, modified from pciSeq algorithm available at https://github.com/kdharris101/iss

LEAD CONTACT AND MATERIALS AVAILABILITY

Further information and requests for resources and reagents should be directed to and will be fulfilled by the Lead Contact, Joakim Lundeberg (joakim.lundeberg@scilifelab.se). This study did not generate new unique reagents.

EXPERIMENTAL MODEL AND SUBJECT DETAILS

Human developmental tissue

Four human developmental heart tissues were used in the study. Post-conceptional and clinical age were determined using clinical ultrasound and stage-dependent anatomical landmarks of the embryos: 4.5-5, 6.5, 6.5-7, and 9 PCW. Samples were collected after elective surgical abortions at the Department of Obstetrics and Gynecology at Karolinska University Hospital, with the written informed consent of the pregnant women. All patients were over 18 years of age and Swedish-speaking. The midwives that informed the patients and the gynaecologists performing the abortions did not participate in the research. Heart tissues were dissected in physiological sodium chloride solution under sterile conditions within an hour of collection. Gender information of the heart tissues was computationally derived. Specifically, hearts at 4.5-5 and 6.5 PCW were male, while the heart at 6.5-7 and 9 PCW were female. Hearts at 4.5, 6.5 and 9 PCW underwent ST and ISS analysis, while the heart at 6.5-7 PCW underwent cell dissociation prior scRNA-seq. The inclusion of first trimester tissue in the study was approved by the Regional Ethical Review Board in Stockholm and the National Board of Health and Welfare. All procedures met the ethical stipulations of the Helsinki Convention (Dnr: 2:9/2015), and all experiments were performed in accordance with relevant guidelines and regulations.

METHOD DETAILS

Experimental design

Replication

Each of the four developmental heart tissues were collected at unique time points, i.e. 4.5-5, 6.5, 6.5-7, and 9 PCW. Samples at 6.5 and 6.5-7 PCW were considered as biological replicates to compared gene expression detected by ST and scRNA-seq.

Consecutive tissue sections from the same heart tissue were considered technical replicates in the ST (Figure S1A) and ISS (Figure 6C; Figure S5B) experiments. However, it is important to notice that consecutive sections are highly similar but not identical.

Strategy for randomization and/or stratification

Not performed.

Blinding at any stage of the study

Not performed.

Sample-size estimation and statistical method of computation

Not performed.

Inclusion and exclusion criteria of any data or subjects

Not performed.

Quality control arrays and spatially barcoded arrays

Arrays for quality control experiments

Codelink-activated microscope glass slides were uniformly coated with poly-T_{20}VN oligonucleotides (IDT, Skokie, IL) over a 6,200 x 6,600 μm area according to the manufacturer's instructions (Figure S1P).

Arrays for spatially barcoded experiment

A total of 1,007 spots with a diameter of 100 μm and unique barcoded oligonucleotides coupled to a poly-T_{20}VN capture region (IDT) were printed onto Codelink-activated glass slides over a 6,200 x 6,600 μm area. All printed spots had a center-to-center distance of 200 μm (Ståhl et al., 2016) (Figure S1Q).

Preparation of human developing hearts

ST and ISS experiments

Heart tissues at 4.5-5, 6.5 and 9 PCW were embedded in Tissue-Tek (OCT) and snap-frozen using an isopentane/dry ice slurry. To enable spatial protein and gene expression analyses, the hearts were cryosectioned at 5 μm thickness and systematically placed either on Superfrost microscope glass slides (Thermo Fisher Scientific) or the prepared Codelink-activated microscope glass slides, after which they were stored at -80°C.

scRNA-seq experiment

The heart tissue at 6.5-7 PCW was divided into two pieces, each of which was minced into smaller pieces using a sterile scalpel. The two samples were then pre-digested overnight at 4°C in Hank's balanced salt solution (HBSS) with 0.5 mg/ml trypsin (Gibco 15090046; Thermo Fisher Scientific, Waltham, MA) according to an established protocol (Månsson-Broberg et al., 2016). The pre-digested heart samples were subsequently treated with collagenase type II (160 U/ml; Worthington Biochemical, Lakewood, NJ) in HBSS for 15 min at 37°C under gentle stirring. The supernatant was centrifuged at 220 × *g* for 8 min and the pellet was

re-suspended in HBSS containing 0.04% BSA (Gibco 15260037). The collagenase digestion was repeated until the tissue was completely dissociated. Cells were re-suspended in HBSS containing 0.04% BSA and kept on ice until library preparation.

Hematoxylin & eosin staining and imaging

Tissue sections mounted on Codelink-activated glass slides underwent fixation at room temperature in neutral formaldehyde solution, diluted 1:10 from 36.5–38.0% stock solution (Sigma-Aldrich, F8775-25ML) in 1×PBS (Medicago, 09-9400). Fixation occurred for 10 min. Next, tissue sections were washed with 1×PBS. Subsequently, glass slides were incubated in Mayer's Hematoxylin (#S3309, Daco) for 7 min, washed in MQ RNase/DNase-free water, incubated in Bluing buffer (#CS702, Dako, Glostrup, Denmark) for 2 min, and then washed in MQ RNase/DNase-free water. Eosin (#HT110216; Sigma Aldrich, St. Louis, MO) staining was then performed using a 1:20 dilution in a 0.45M Tris and 0.5M acetic acid solution (pH 6.0). The tissue sections were left to dry at room temperature and then incubated for 5 min at 37°C. Bright field imaging was performed with the Metafer Slide Scanning platform (Metasystem, Altlussheim, Germany) and images were stitched together using VSlide (Metasystem).

Immunohistochemistry

Tissue sections mounted on Superfrost microscope glass slides were fixed in 4% formaldehyde and incubated in blocking solution containing 5% serum in PBS for 30 min. Next, the slides were incubated overnight in blocking solution containing two *primary antibodies*: Anti-Cardiac Troponin T antibody [1C11] ab8295 (Abcam, Cambridge, United Kingdom) IgG1, 1:600, and Anti-Actin α-Smooth Muscle antibody A2547 (Sigma Aldrich) clone 1A4, IgG2a, 1:250. After washing, the slides were incubated for two hours in blocking solutions containing the *secondary antibodies* Sek Goat-anti-Mouse IgG1, Alexa Fluor® 488 A-21121, 1:600 (Thermo Fischer Scientific), and Sek Goat anti-Mouse IgG2a, Alexa Fluor® 568 A-21134, 1:600 (Thermo Fischer Scientific).

The glass slides were counterstained with 4,6-diamidino-2-phenylindole (DAPI) (Molecular probe, D21490; Thermo Fisher Scientific) and mounted using Vectashield mounting medium (VEH-1000; Vector Laboratories, Burlingame, CA). Images were captured using a Nikon A1-R confocal microscope (Nikon Corporation, Tokyo, Japan) fitted with a 20x/0.75 air objective with tiling to increase the field of view. Three different images were acquired to visualize proteins. The blue and red images were acquired simultaneously, after which the green image was acquired to avoid bleed through. Additional images were acquired without saturation and/or underexposure.

Specific optimizations of the ST protocol for developmental heart tissue

ST conditions for tissue sections from hearts at 4.5, 6.5 and 9 PCW were optimized using quality control arrays (Figure S1P). Due to differences in tissue size, the permeabilization treatment times were identified as 9, 12, and 13 min for the heart tissues at 4.5-5, 6.5, and 9 PCW, respectively. Subsequently, the optimized parameters were applied to the tissue sections on the spatially barcoded arrays (Figure S1Q) to generate ST libraries. Tissue permeabilization was performed with pepsin (Sigma Aldrich, P7000-25G) 0.1%/0.1 M HCl (Fluka, 318965-500 ML).

Library preparations and sequencing

Libraries were prepared using either a manual library preparation protocol (Ståhl et al. 2016) or a previously described automated MBS 8000+ system (Jemt *et al.*, 2016).

ST experiments - manual

Glass slides with tissue sections attached to arrays for spatially barcoded experiments were put in ArrayIT mask holders (ArrayIT Corporation, AHC1X16) to obtain reaction chambers for each array and perform on-array reactions. Tissue sections were treated with 70 μl of 1× Exonuclease I Reaction Buffer (NEB, Bionordika, B0293S), diluted in Milli-Q DNase/RNase free water, with 0.19 μg/μl BSA (NEB, Bionordika, B9000S) at 37°C for 30 min. After washing each array with 100 μl of 0.1× SSC (Sigma-Aldrich, s6639-1L) diluted with Milli-Q DNase/RNase free water (standard washing), 70 μl of permeabilization solution (see "Specific optimizations of the ST protocol for developmental heart tissue") were added to each array chamber and incubated at 37°C for the time described at the previous paragraph "Specific optimizations of the ST protocol for developmental heart tissue". The solution was washed away as described above, and 70 μl of reverse transcription mixture in Milli-Q DNase/RNase free water was added to each of the array chambers. The reverse transcription mixture was incubated at 42°C overnight and contained: 1× First Strand Buffer (Thermo Fisher, included in Superscript III 4-pack), 5 mM DTT (Thermo Fisher, included in Superscript III 4-pack), 0.5 mM of each dNTP (Thermo Fisher, R0191), 0.19 μg/μl BSA, 50 ng/μl actinomycin D (Sigma-Aldrich, A1410-2MG), 1% DMSO (Sigma-Aldrich, 472301), 20 U/μl Superscript III (Thermo Fisher, 18080085) and 2 U/μl RNaseOUT (Thermo Fisher, 10777019).

Before releasing the probes from the array surface, array chambers underwent standard washing steps, and tissue sections were degraded by adding 70 μl of a 3:100 mixture of β-mercaptoethanol (Calbiochem, 444203) and RLT buffer (Qiagen, 79216), respectively, to each array. The reaction was incubated at 56°C for 1h and 30min at 300 rpm. Next, the mixture was pipetted out and array chambers underwent standard washing step. Then, 70 μl mixture containing 20 μl Proteinase K (Qiagen, 19131) for each 140 μl PKD buffer (Qiagen, 1034963) were added to the array chambers for incubation at 56°C for 1 h at 300 rpm interval shaking. At the end of the incubation, the mixture was pipetted out and array chambers underwent standard washing step. Afterwards, the glass slides were removed from the ArrayIT mask holders and washed in 2× SSC, which contained 0.1% SDS (Sigma-Aldrich), at 50°C for 10 min, and subsequently washed in 0.2× SSC and 0.1× SSC at room temperature for 1 min. At this

point, glass slides were again put in clean ArrayIT mask holders to release the mRNA–cDNA hybrids from the array surface. The probe release was performed by adding 70 μl of release mix to the array chambers. The release mix was composed of 1.1× Second Strand Buffer (Thermo Fisher, 10812014), 8.75 μM of each dNTP, 0.20 μg /μl BSA, and 0.1 U/μl USER enzyme (NEB, Bionordika, M5505L). Incubation was performed at 37°C for 2h. At the end of the incubation, 65 μl of the released probes mixture were collected from each array chamber. Subsequently, a second strand cDNA synthesis was performed by adding 5 μl to each sample. The mixture was as follows: 2.7× First Strand Buffer, 3.7 U/μl DNA polymerase I (Thermo Fisher, 18010025) and 0.18 U/μl RNaseH (Thermo Fisher, 18021071), and the reaction was incubated at 16°C for 2 h. Then, 5 μl of T4 DNA polymerase (NEB, Bionordika, M0203L) were added to each samples for an additional incubation at 16°C for 20 minutes. Next, 25 μl of 80 mM EDTA (Thermo Fisher, 15575-020) were added to each sample before purification with Agencourt RNAClean XP beads (Beckman Coulter, A63987) following the manufacturer's instructions. Elution was performed with Milli-Q DNase/RNase-free water. Afterwards, samples underwent *in vitro* transcription (IVT), which mixture contained 1× T7 Reaction Buffer (Ambion, AM1334), 7.5 mM of each NTP (Ambion, AM1334), 1× T7 Enzyme Mix (Ambion, AM1334) and 1 U/μl SUPERaseIN (Ambion, AM2694) in a final volume of 10.4 μl per sample. From this mixture, a total of 5.6 μl were added to each purified sample and the reaction was incubated for 37°C for 14 h. Subsequently, a second purification was performed on the amplified RNA (aRNA) using the Agencourt RNAClean XP beads following the manufacturer's instructions, and elution was performed in 10 μl of Milli-Q DNase/ RNase-free water. Next, a ligation reaction containing 8 μl of aRNA and 2.5 μl of ligation adapter (IDT, [rApp]AGATCGGAAGAGCACACGTCTGAACTCCAGTCAC[ddC]) was incubated at 70°C for 2 min. Then, 4.5 μl of the ligation mixture were added to each sample, thus obtaining a final composition of 1× T4 RNA Ligase Reaction Buffer (NEB, M0242L), 20 U/μl T4 RNA Ligase2 truncated (NEB, M0242L), 4 U/μl RNase Inhibitor Murine (NEB, M0314L) and 0.5 μM ligation adapter. Samples were incubated at 25°C for 1 h and then purified using Agencourt RNAClean XP beads according to the manufacturer's instructions. Elution was performed in 10 μl of Milli-Q DNase/RNase-free water. Subsequently, a reverse transcription (RT) reaction was set up by adding to the eluted samples: i) a primer (IDT, 5′-GTGACTGGAGTTCAGACGTGTGCTCTTCCGA-3′) at a final concentration of 1.7 μM; ii) 1 μl of dNTPs (0.83 mM final concentration of each μl dNTP). These were incubated at 65°C for 5 min and then placed on ice. Next, 8 μl of a RT reaction mixture (final concentration: 1× First Strand Buffer, 0.05 M DTT, 500 μM each dNTP, 1 mM RT-primer, 10 U/μl Superscript III, 2 U/μl RNaseOUT) were added. Incubation was performed at 50°C for 1 h. Then, samples were purified using Agencourt RNAClean XP beads according to the manufacturer's instructions, and eluted in 10 μl of Milli-Q DNase/ RNase-free water.

To identify the optimal number of PCR cycles for final library amplification a qPCR was performed in 10 μl of final volume. Specifically, the reaction mixture contained 2 μl of purified sample, 1× KAPA HiFi HotStart Readymix (KAPA Biosystems, KK2602), 0.5 μM PCR InPE1.0 primer (Eurofins, 5′-AATGATACGGCGACCACCGAGATCTACACTCTTTCCCTACACGACGCT CTTCCGATCT-3′), 0.01 μM PCR InPE2.0 primer (Eurofins, 5′-GTGACTGGAGTTCAGACGTGTGCTCTTCCGATCT-3′), 0.5 μM PCR Index primer (Eurofins, 5′-CAAGCAGAAGACGGCATACGAGATXXXXXXGTGACTGGAGTTC-3′), and 1× EVA green (Biotium, 31000). The programme was as follows: 1×, 98°C 3 min; 25×, 98°C 20 s, 60°C 30 s, 72°C 30 s. Instead, the final PCR was performed in a final volume of 25 μl with the above programme including a final extension at 72°C for 5 min and the number of cycles identified by qPCR. The final libraries were purified by an automated MBS robot and eluted in 20 μl of Elution Buffer (Qiagen, 19086). The final library concentration was assessed using the Qubit HS Assay Kit (Life Technologies, Q32852) and the average length was measured using the DNA 1000 kit (Agilent, 5067-4626) on a 2100 Bioanalyzer (Agilent, G2939BA) following the manufacturer's instructions. Afterwards, libraries were diluted to 4 nM and underwent paired-end sequencing on an Illumina NextSeq platform according to the manufacturer's instructions. 31 bases from read 1 were used to determine the spatial barcode and the unique molecular identifier (UMI), and 121 bases from read 2 were used to cover the genetic region. Each tissue section generated 35-106 million raw reads and covered 56 - 245 spots (Table S1A).

ST experiments - automated

Glass slides with tissue sections attached to arrays for spatially barcoded experiments were treated as described in the above section, i.e. "Library preparations and sequencing/ST experiments - automated", up to the end of the probe release incubation with subsequent collection of 65 μl released probes mixture. Then, the released samples were loaded onto a Nordiag Magnatrix 8000+ system to perform in an automated fashion the following steps: i) second strand cDNA synthesis; ii) sample purification with Agencourt RNAClean XP beads; iii) IVT; iv) sample purification with Agencourt RNAClean XP beads; v) adapter ligation; vi) sample purification with Agencourt RNAClean XP beads; vii) reverse transcription; viii) sample purification with Agencourt RNAClean XP beads. The automated procedure was divided in two parts, which were run on the same instrument. Part 1 consisted of steps i-iv, while part 2 consisted of steps v-viii. Scripts to run the automated system can be found at https://github.com/jemten/MBS. Reaction volumes and reagent concentrations are as reported in the section "Library preparations and sequencing/ST experiments – automated", with the exception of the first sample purification with Agencourt RNAClean XP beads after second strand cDNA synthesis. Here, samples were eluted in a 12 μl 40 mM nucleotide solution. At the end of the automated protocol part 2, samples followed the preparation and sequencing described in "Library preparations and sequencing/ST experiments – manual".

scRNA-seq experiments

The two cellular suspensions (preparation described in the section "*Preparation of human developing hearts"*) were loaded into two separate wells (estimated loading of 3,000 cells/well) in a 10x Chromium instrument (10X Genomics, Pleasanton, CA) using the Single Cell 3' v2 reagent kit according to the manufacturer's instructions. Paired-end sequencing was then performed on a HiSeq2500 instrument (Illumina, San Diego, CA) using the following read lengths: 26 bases for read 1 (cell barcode and UMI), 8 bases for the I7

index (sample index), and 98 bases for read 2 (transcript information). Each cellular fraction (1,979 and 2,047 cells per fraction) generated about 155 million raw reads, corresponding to ~77,000 reads per cell (Table S1B).

Image alignment of ST tissue and spots

After probe release from the ST barcoded arrays, 70 μl of a hybridization mixture [0.96x PBS, 0.2 μM Cy3 anti-A probe (Eurofins, [Cy3] AGATCGGAAGAGCGTCGTGT), and 0.2 μM Cy3 anti-frame probe (Eurofins, [Cy3]GGTACAGAAGCGCGATAGCAG) was added, and the glass slides were incubated for 10 min at room temperature. Glass slides were then washed in 2x SSC containing 0.1% SDS for 10 min at 50°C and then in 0.2x SSC and 0.1x SSC for 1 min each at room temperature. Fluorescence imaging was performed using the Metafer Slide Scanning platform and images were stitched together using the VSlide software. Bright field images of the tissue sections and fluorescence images of the spot positions were manually aligned using Adobe Photoshop CS6 (Adobe, San Jose, CA).

Rolling circle amplification (RCA) and *in situ* sequencing (ISS)

RCA and ISS were performed using procedures similar to those reported by Ke et al. (Ke et al., 2013). Briefly, tissue sections mounted on Superfrost microscope glass slides were fixed (3.7% w/v paraformaldehyde in DEPC-PBS, at 22°C for 5 min) and washed with DEPC-PBS. For permeabilization, samples were treated with 0.01% pepsin (Sigma) in 0.1M HCl at 37°C for 1.5 min and washed twice in DEPC-PBST for 2 min. Tissues on slides were then covered with Secure-Seal hybridization chambers (Invitrogen) for the following experiment. Reverse-transcription was performed on the slides overnight in a reaction mixture containing 5 μM of unmodified random decamers, 500 μM dNTPs (Fermentas), 0.2 μg/μl BSA (NEB), 20 U/μl of TranscriptMe reverse transcriptase (Gdansk), 1 U/μl RiboLock RNase Inhibitor (Fermentas), and 1× TranscriptMe reaction buffer. Padlock probes were designed for 69 genes based on the ST and scRNA-seq analyses; their sequences are listed in Table S4B. After reverse transcription and two washes with DEPC-PBS-T (0.1% Tween-20), tissues were post-fixed in 3.7% (w/v) paraformaldehyde in DEPC-PBS for 30 min at room temperature. RNA degradation was then performed, followed by hybridization of the padlock probes and their ligation on synthesized cDNA. A mix containing 10 nM of each padlock probe, 50 μM dNTPs, 0.4 U/μl RNase H (Fermentas), 0.5 U/μl Ampligase, 20% formamide, 50 mM KCl, and 1× Ampligase buffer (10 mM $MgCl_2$, 25 mM KCl, 0.5 mM NAD and 0.01% Triton X-100, 20 mM Tris-HCl, pH 8.3) was added to the sample reaction chambers on the slides. The slide was incubated at 37°C for 30 min, and 45°C for 45 min before washing twice with 1× DEPC-PBS-T. For RCA, an RCA mix (1 U/μl phi29 polymerase (Fermentas), 1× phi29 polymerase buffer, 0.25 mM dNTPs, 0.2 μg/μl BSA and 5% glycerol in DEPC-H_2O) was added to the reaction chamber and incubated overnight at 30°C. Secure-Seal hybridization chambers were removed, and the RCA products (RCPs) were sequenced using sequencing by ligation chemistry. Images were acquired using an Axioplan II epifluorescence microscope (40× Plan-Apochromat /1.4 NA Oil objective) with a motorized stage (WSB Z-Piezo) and metal halide lamp. After imaging, the labeled RCPs were stripped by UNG treatment and stringent washing, and the hybridization, ligation and imaging processes were repeated. Four rounds of sequencing were performed in total. Finally, a hybridization round using anchor primer and interrogation probes for selected targets were performed as described for the previous round.

Single-molecule fluorescent *in situ* hybridization (smFISH)

Individual probes were produced using an adapted procedure for generating smFISH probes for MERFISH (Moffitt and Zhuang, 2016) as described in iFISH (Gelali et al., 2019). Essentially, every probe consists of between 26 to 100 unique oligonucleotides, each of which targets 30 nucleotides of the corresponding protein-coding sequence. A complete list of the oligonucleotide sequences of each probe is provided in Table S4D. For smFISH, we fixed tissue sections mounted on Superfrost microscope glass slides by immersing the slide in a freshly prepared mixture of methanol and acetic acid (3:1 v/v) for 15 min at room temperature. For hybridization, we followed a recently described two-step procedure (Gelali et al., 2018). Images were captured using a 60X oil immersion objective mounted on an inverted epifluorescence microscope (Eclipse Ti-E, Nikon) equipped with an EMCCD camera (iXON Ultra 888, ANDOR, Belfast, United Kingodm) and controlled using NISElements (Nikon). We used custom-built software written in MATLAB to process the images and localize mRNA molecules.

QUANTIFICATION AND STATISTICAL ANALYSIS

No methods were used to determine whether the data met assumptions of the statistical approaches utilized in the following analyses.

Sequence alignment and annotation

ST experiments

ST sequencing data were processed using an automated ST Pipeline (version 1.6.0, mode: multi-mapping disabled and no ambiguously annotated reads allowed) (Navarro et al., 2017). Reads were mapped against the human genome (ENSEMBL genome assembly GRCh38, release 86) using STAR (version 2.4.2a, mode: two-pass; https://github.com/alexdobin/STAR/tree/STAR_2.4.2a) (Dobin et al., 2013). Mapped reads were annotated using htseq-count (version 0.10.0, mode: union) (Anders et al., 2015)

with GENCODE gene annotations for the GRCh38 genome assembly (GENCODE release 25). Mapped and annotated reads were demultiplexed into array coordinates from the spatial barcodes located in the corresponding forward reads using a python implementation of the TagGD tool (Costea et al., 2013).

scRNA-seq experiments

Single-cell sequencing data were processed using the CellRanger pipeline (version 2.1.1; 10X Genomics). Reads were mapped against the human genome (ENSEMBL genome assembly, release 86) and annotated with GENCODE gene annotations for the GRCh38 genome assembly (GENCODE release 25).

Data quality and filtering

ST experiments

The count matrix was first enriched for protein-coding RNA and lincRNA gene types. Next, the expression matrix was filtered by removing MALAT1 and MTRNR genes, as well as highly expressed genes related to hemoglobin (because extracting the hearts from the bodies caused considerable variation in their blood contents). Additionally, highly expressed Y-chromosome linked genes were removed because the heart tissue samples represented both genders (Table S1C). Spots with fewer than 500 genes and genes expressed in fewer than 15 spots were excluded the joint analysis of the three post-conception time points. Spots with over 10% mitochondrial gene expression were also discarded. Statistical details of the joint analysis can be found at the section ''Spatiotemporal gene expression dynamics during human heart development'' of Results, and in Figure S1B–S1J.

scRNA-seq experiments

The single-cell count matrix was first enriched for protein-coding RNA and lincRNA gene types, after which the genes removed in the analysis of the ST samples were excluded (Table S1C). Cells with fewer than 500 genes and genes expressed in fewer than 15 cells were excluded from the analysis. Cells with over 20% mitochondrial gene expression were also discarded. Doublets were discarded using DoubletFinder (McGinnis et al., 2019) (version 1.0.0; https://github.com/chris-mcginnis-ucsf/DoubletFinder), with an expected multiple rate of ~1.6% (according to 10X Genomics guidelines) (Figure S3C). Statistical details of this analysis can be found at the section ''Single-cell gene expression analysis of a 6.5-7 PCW human embryonic heart'' of Results.

Data processing

ST experiments

Normalization, dimensionality reduction and clustering of ST data were performed jointly on spots from all three post-conception time points. The approach were implemented using the Seurat package (version 2.3.4; https://satijalab.org/seurat/install.html) (Satija et al., 2015) with a scale factor defined as the average of column sums across the expression matrix and using the LogNormalize method. Genes with high dispersion were selected using the FindVariableGenes function (settings: mean.function = ExpMean, dispersion.function = LogVMR, x.low.cutoff = 0.1, x.high.cutoff = 10, y.cutoff = 0.5). Sources of technical and biological variability within the data, including cell cycle activity (Kowalczyk et al., 2015) and number of genes and mitochondrial content were regressed out using the ScaleData function. Independent component analysis (ICA) was performed on the highly dispersed genes and the seven significant components for use in downstream analyses were determined by visualizing ICA vectors as heatmaps on the tissue sections. Clusters were then identified using the FindClusters function (settings: reduction.type = "ica", seven significant ICA vectors, k.param = 30, resolution = 0.8).

Statistical details of this analysis can be found at the section ''Spatiotemporal gene expression dynamics during human heart development'' of Results and Figure 2D.

scRNA-seq experiments

Normalization, dimensionality reduction, and clustering of scRNA-seq data were performed using the Seurat package (version 2.3.4) (Satija et al., 2015), and genes with high dispersion were selected using the FindVariableGenes function (settings: mean.function = ExpMean, dispersion.function = LogVMR, x.low.cutoff = 0.2, x.high.cutoff = 10, y.cutoff = 0.5). Cell cycle activity (Kowalczyk et al., 2015), number of genes, and mitochondrial content across the data were regressed out using the ScaleData function. Principal component analysis (PCA) was performed on the 20 most significant components as determined by the PCElbowPlot function, showing the standard deviation of the principal components. Clusters were identified using the FindClusters function (settings: reduction.type = "pca", dims.use: 1:20, k.param = 30, resolution = 0.7). Statistical details of this analysis can be found at the section ''Single-cell gene expression analysis of a 6.5-7 PCW human embryonic heart'' of Results and in Figure 3B.

Cluster visualization and differential gene expression analysis

We used t-distributed Stochastic Neighbor Embedding (tSNE) to visualize single-cell and ST clusters in a reduced 2D space. To identify differentially expressed genes, pair-wise comparisons of individual clusters against all other clusters were performed using the FindAllMarkers function (settings: min.pct = 0.25, thresh.use = 0.25) in the Seurat package (version 2.3.4) (Satija et al., 2015). Statistical details of the differential gene expression analysis on ST clusters can be found at the section ''Spatiotemporal gene expression dynamics during human heart development'' of Results and in Figures 2D and 2H and Table S2. Statistical details of the clusters identified in the single-cell data can be found at the section ''Single-cell gene expression analysis of a 6.5-7 PCW human embryonic heart'' of Results and in Figure 3B and Table S3.

Gene ontology enrichment of gene clusters

GO characteristics of gene clusters were determined using the clusterProfiler package (version 3.8.1) (Yu et al., 2012) for all DE genes with an average logFC value above zero, and an adjusted p value below 0.01. The compareCluster function was used with a pvalueCutoff = 0.05. Statistical details of this analysis can be found at the sections ''Spatiotemporal gene expression dynamics during human heart development'' and ''Disentangling cell-type similarities by spatial analysis'' of Results and in Figure S2A and Figure S6B.

Bulk treated ST and single-cell data

Pair-wise comparisons between samples were performed on aggregated counts from all spots within individual tissue sections or aggregated counts from all the analysed single cells (which can be compared to RNA-seq data). Genes presented in Table S1C, as well as those not detected in either sample, were removed. Scatterplots showing Pearson correlation coefficients were created using log-transformed raw read counts after adding a pseudocount of 1. Statistical details of this analysis can be found at the sections ''Single-cell gene expression analysis of a 6.5-7 PCW human embryonic heart'' of Results and in Figures S1D–S1J and Figure 3A.

ISS image analysis, decoding and single cell analysis

After imaging, sequence decoding was performed as described previously (Ke et al., 2013). Briefly, a stack of images at different focal depths were merged and stitched using Zeiss AxioVision software. Cell nuclei were segmented based on the intensity of the DAPI staining, and cytoplasm was delineated by watershed segmentation. The general stain image (Alex750) for RCPs was enhanced using a top-hat filter before segmentation. After image alignment, the fluorescence intensity from RCP signals representing A, T, C, and G was extracted. The optimal transformation for a merged image of all signals (A + T + C + G) and the general stain was determined based on intensity (Qian et al., 2019). Analysis was performed using CellProfiler (2.1.1, 6c2d896), with called ImageJ plugins from Fiji for image registration. A Matlab (MathWorks, version R2018a) script was used to decode intensity. Each RCP was assigned to a base (A, T, C or G) based on the maximum intensity in all hybridization steps. Quality scores were extracted for all bases, and the lowest quality value determined for any base in a was defined as that transcript's quality. Statistical details of this analysis can be found at the sections ''Creating a cellular gene expression map of the developing heart'' of Results and in Figures 5A, 5C, 5E, S4D, and S5A, and in Tables S4A-S4C.

For single cell analysis, the DAPI images were sliced into smaller images and nuclear segmentation was performed with CellProfiler (multi-threaded), using both DAPI intensity and shape (watershed transformation) as criteria. The identified nuclei were then expanded to 20 pixels to represent cell area. Cells cut by tiling lines were later identified and merged using a custom Matlab script.

Probabilistic spatial cell map based on ISS data

Gene reads were assigned to cells and cells were classified by a probabilistic cell mapping method (pciSeq) that generates spatial maps of cell types defined by scRNA-seq (Qian et al., 2019). The algorithm was initiated by assigning reads to cells based on the overlap between read location and segmented cell area, and assuming equal priors for all cell types plus a prior of 0.5 for type ''zero'' (indicating a cell not belonging to any known class). Two erythrocyte classes (scRNA-seq clusters 6 and 11) and immune cells (cluster 13) were excluded in the mapping procedure. The genes *COL2A1* and *SPARC* were also excluded from mapping due to their spread expression across many cell types. After cell classification, a spatial map of cell types was created using only data for cells with at least five reads each. Each cell was represented as a pie chart of probabilities matching the scRNA-seq clusters, with size proportional to the number of reads assigned to each cell. Statistical details of this analysis can be found at the sections ''Creating a cellular gene expression map of the developing heart'' of Results and in Figure 5B, 5D, Figure 6G, and Figure S6A.

Constructing a reference atlas of a human embryonic heart

Our atlas is based on a previously published human embryonic reference atlas on Carnegie stage 18 (de Bakker et al., 2016), CS18-6524. The heart was cropped out from the rest of the atlas by creating a bounding box with the pixel coordinates (7, 170, 775, 1239). Discrepancies resulting from the cutting plane were corrected for by systematically elongating the heart; the axis was extended by bicubic interpolation using a factor of 3.25. We delimited the embryonic heart into eight anatomical regions based on their annotations; right ventricle, left ventricle, right atrium, left atrium, OFT, ascending aorta, pulmonary trunk and arteries, and epicardium (Figure S7). Regions not covered by the annotations are referred to as ''whole heart''. We noticed that the definition of epicardium in the atlas differed from ours: we would refer to this region as the AV subepicardial mesenchyme, but for consistency we chose to retain the atlas nomenclature in Figure S7D. Each anatomical region is represented in the two-dimensional plane using vector graphics. Image processing for atlas registration relied on custom code written in C++ and R using OpenCV. Bright field images of tissue sections were converted to grayscale and the tissue outline was segmented by applying eight linearly spaced binary thresholds to the intensity data and then using a connected components algorithm with subsequent filtering of components based on size, eccentricity, and intensity (Fürth et al., 2018). Registration of the heart atlas onto each section followed a scheme previously used for brain tissue (Fürth et al., 2018). Contours of both the bright field images of tissue sections and the atlas section were reduced and matched using principal component analysis. Any registration errors were manually corrected by changing, adding or removing landmarks along the contour. The registration transform was obtained by thin-plate B-splines (Bookstein, 1989). Statistical details of this analysis can be found at the sections ''Disentangling cell-type similarities by spatial analysis'' of Results and in Figure 7 and Figure S7.

DATA AND CODE AVAILABILITY

ST and scRNA-seq experiments

The accession number for the raw sequencing data reported in this paper is European Genome-phenome Archive (EGA): EGAS00001003996. Details of the ST analysis pipeline can be found at https://github.com/SpatialTranscriptomicsResearch/st_pipeline.

Count matrices are available at https://www.spatialresearch.org.

Data S1. High-resolution histological images with cluster coordinates, Related to Figure 2, is available on Mendeley: https://data.mendeley.com/datasets/zkzvyprd5z/draft?a=c3021f62-a7af-4824-b89d-d7fbfec67902. Individual high-resolution bright field images with cluster coordinates of 19 tissue sections from the 4.5-5 PCW (four tissue sections), 6.5 PCW (nine tissue sections) and 9 PCW (six tissue sections) hearts.

ISS experiments

ISS image data are available at https://doi.org/10.6084/m9.figshare.10058048.v1. Matlab script to decode intensity information is available at https://github.com/Moldia/in_situ_seq.

The scripts for data analysis are available at https://github.com/Moldia/heart, modified from pciSeq algorithm available at https://github.com/kdharris101/iss.

Human embryonic heart atlas

Source code and scripts used to analyze data are available upon request.

Details of the human embryonic heart atlas can be found at https://github.com/MickanAsp/Developmental_heart.

ADDITIONAL RESOURCES

We provide a web resource, which allows visual exploration of our datasets, i.e., ST, scRNA-seq, ISS, and 3D atlas. The web resource is part of the Swedish Human Developmental Cell Atlas initiative and give access to: i) the single-cell RNA-seq and Spatial Transcriptomics viewer, a Shiny application to visualize genes of interest in scRNA-seq and ST clusters with anatomical definitions; ii) *in situ* sequencing cell mapping visualization of reads and probabilistic cell type assignments; iii) 3D Viewer to explore genes of interest in the 3D heart structure. The web resource can be accessed at https://hdca-sweden.scilifelab.se/a-study-on-human-heart-development/.

Supplemental Figures

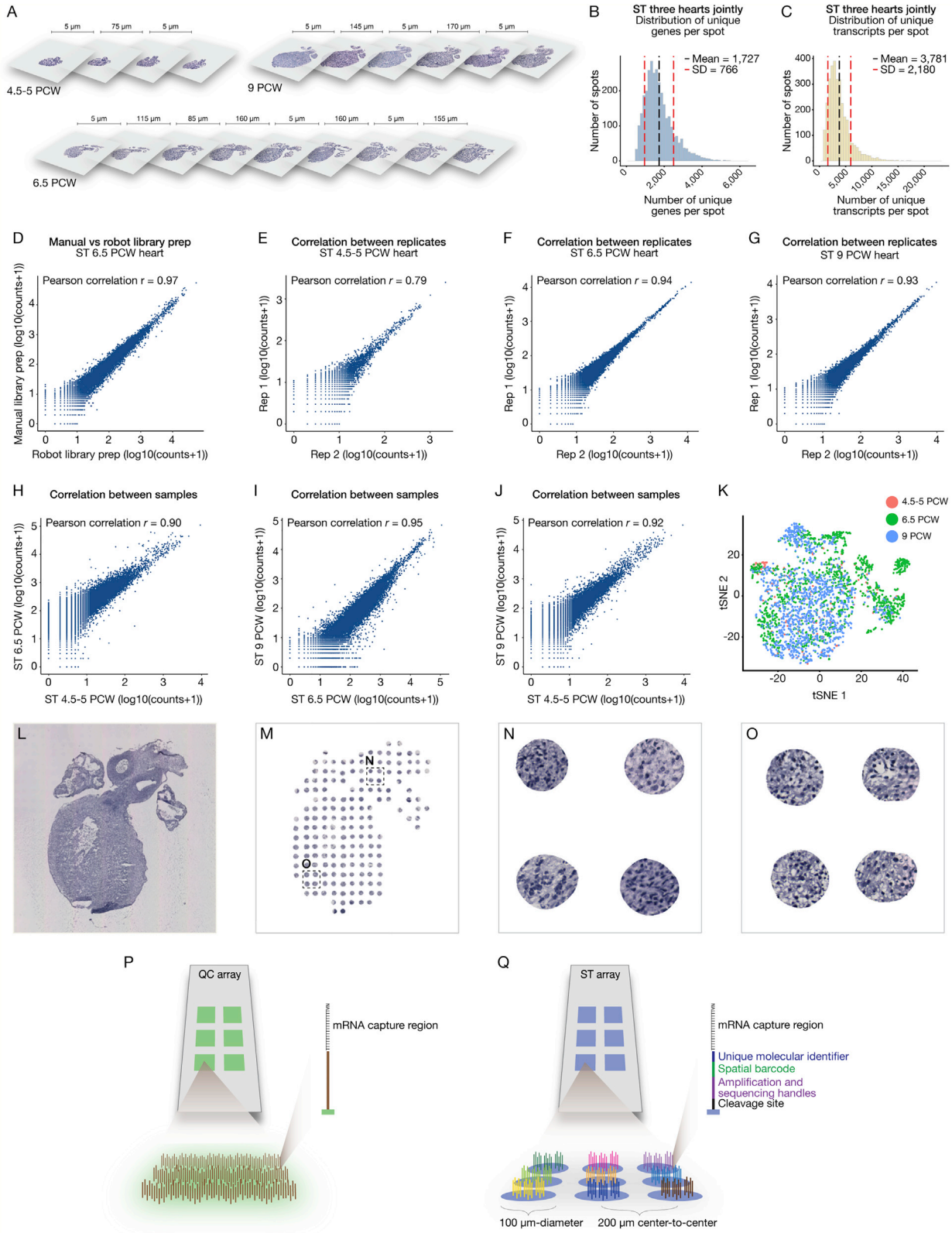

(legend on next page)

Figure S1. Overview of ST Samples Included in this Study, Related to Figure 2

(A) Distance between tissue sections in the 4.5-5, 6.5, and 9 PCW human embryonic hearts included in the ST analysis. Sections are shown in the dorsal (left-most) to ventral direction (right-most).

(B-C) Distributions of the number of genes (B) and transcripts (C) detected per spot in the three hearts. Black dashed lines indicate mean values while the red dashed lines indicate the standard deviation.

(D) Scatterplot showing the Pearson correlation of gene expression levels detected in tissue sections of the 6.5 PCW heart, from which libraries were prepared either manually or automatically. The plot demonstrates that there is no technical variation between the two methodologies. The analysis was conducted by aggregating the spot information across corresponding sections.

(E-G) Scatterplots showing Pearson correlation of the gene expression detected in consecutive tissue sections from the three hearts. The correlation between sections of the 4.5-5 PCW heart was slightly lower than what was observed for the other hearts, probably due to the smaller size of the heart, which resulted in less data points (i.e. spots). The analysis was conducted by aggregating the spot information across corresponding sections.

(H-J) Scatterplots showing Pearson correlation of the gene expression detected among the three hearts (i.e., 4.5-5, 6.5, and 9 PCW). The analysis was conducted aggregating the spot information across corresponding samples.

(K) tSNE plot shown in Figure 2D, here colored by developmental time point.

(L) A hematoxylin and eosin stained tissue section from the 6.5 PCW heart sample.

(M) Tissue domains above spot positions.

(N-O) Magnified images of the marked sets of spots from (M), showing approximately 20-40 cells per spot.

(P) For quality control experiments, six sub-arrays are uniformly coated (green area) with reverse-transcription oligo-dT primers. Thin developmental cardiac tissue sections are placed on top of each sub-array and fluorescent nucleotides are thereafter incorporated during cDNA synthesis. This allows for visualization of gene expression and optimization of permeabilization treatment times.

(Q) For ST experiments, 1,007 individual spots (blue area) are printed with reverse-transcription oligo-dT primers. Here, primers are linked to a unique oligo-nucleotide sequence (i.e. spatial barcode) specific to the spot's position.

(L and M) Figures contain tiled images to cover the entire tissue.

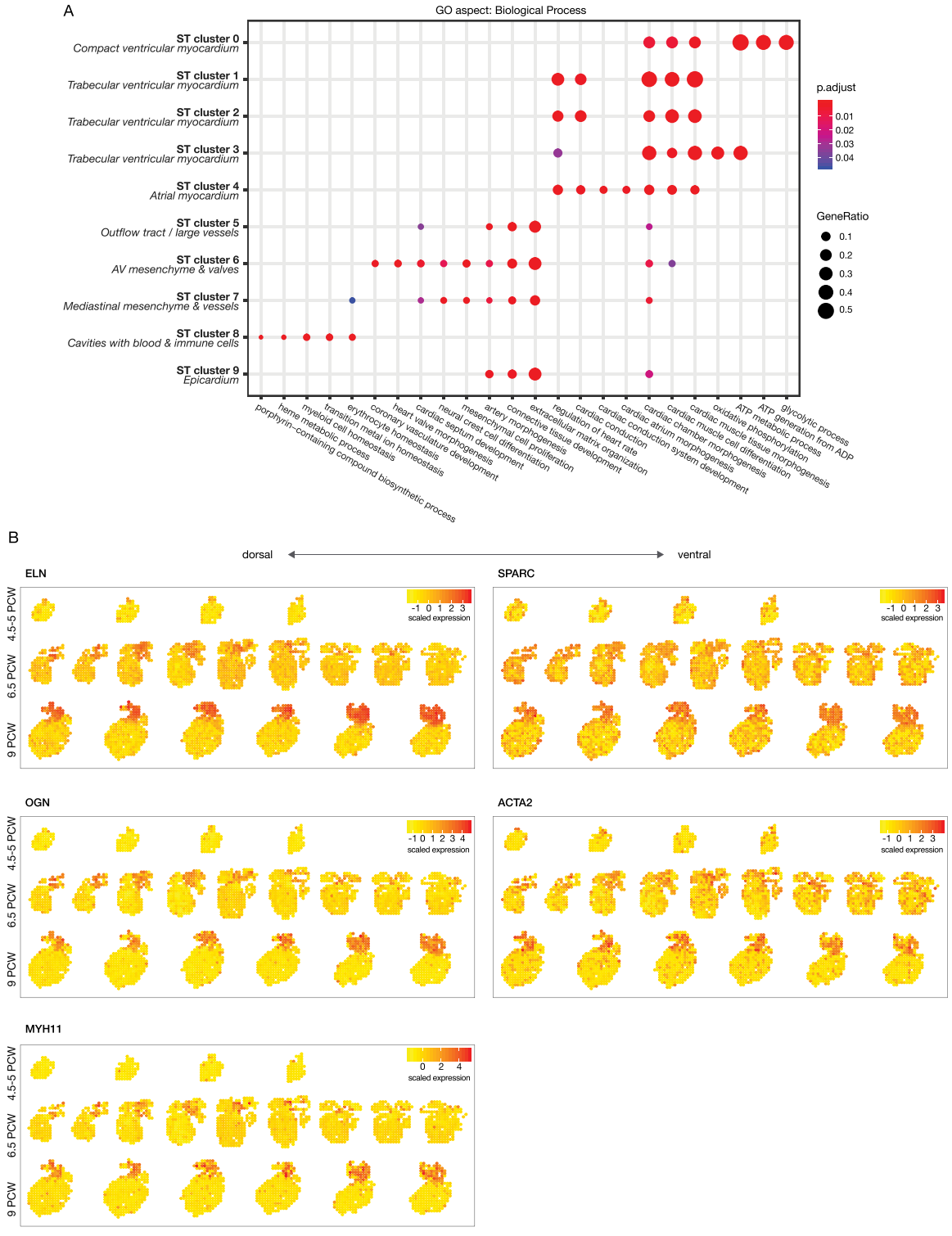

Figure S2. ST Gene Expression Features, Related to Figure 2

(A) Gene ontology annotations of upregulated genes with adjusted p value lower than 0.05 across heart biological processes. The dots in the dotplot indicate the GO categories in which ST clusters are more likely to have biological meaning. The color of dots indicates high (red) or low (blue) enrichment for a specific GO category. The size of dots displays the overlap between the input gene lists with the collection of gene sets.

(B) Spatially resolved heatmaps across tissue sections from the three individual hearts, showing spatial gene expression patterns of *ELN*, *SPARC*, *OGN*, *ACTA2*, and *MYH11*.

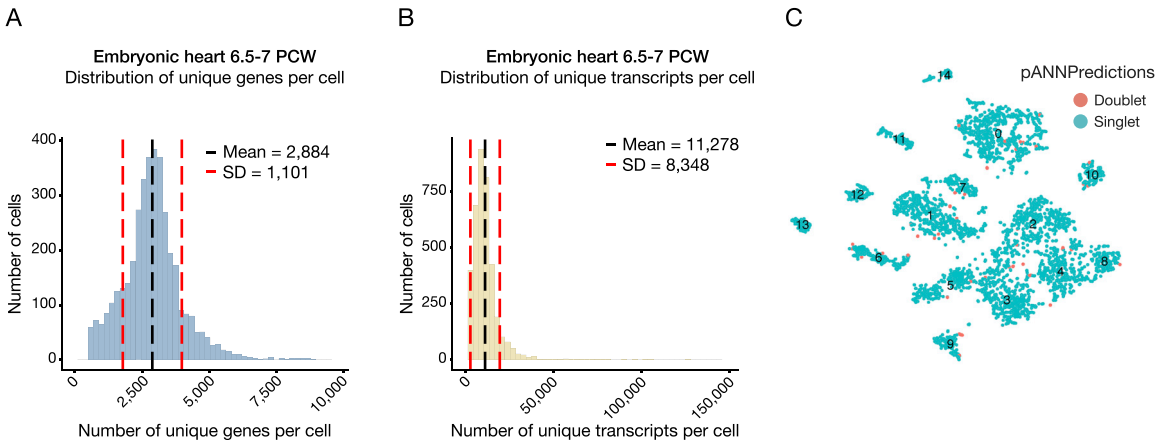

Figure S3. scRNA-Seq Data of the 6.5-7 PCW Heart, Related to Figure 3

(A-B) Distribution of the number of genes (A) and transcripts (B) detected per cell. Black dashed lines indicate mean values while the red dashed lines indicate the standard deviation.

(C) tSNE plot shown in Figure 3B, but colored based on cell doublet and singlet information. Doublets were discarded before down-stream analyses.

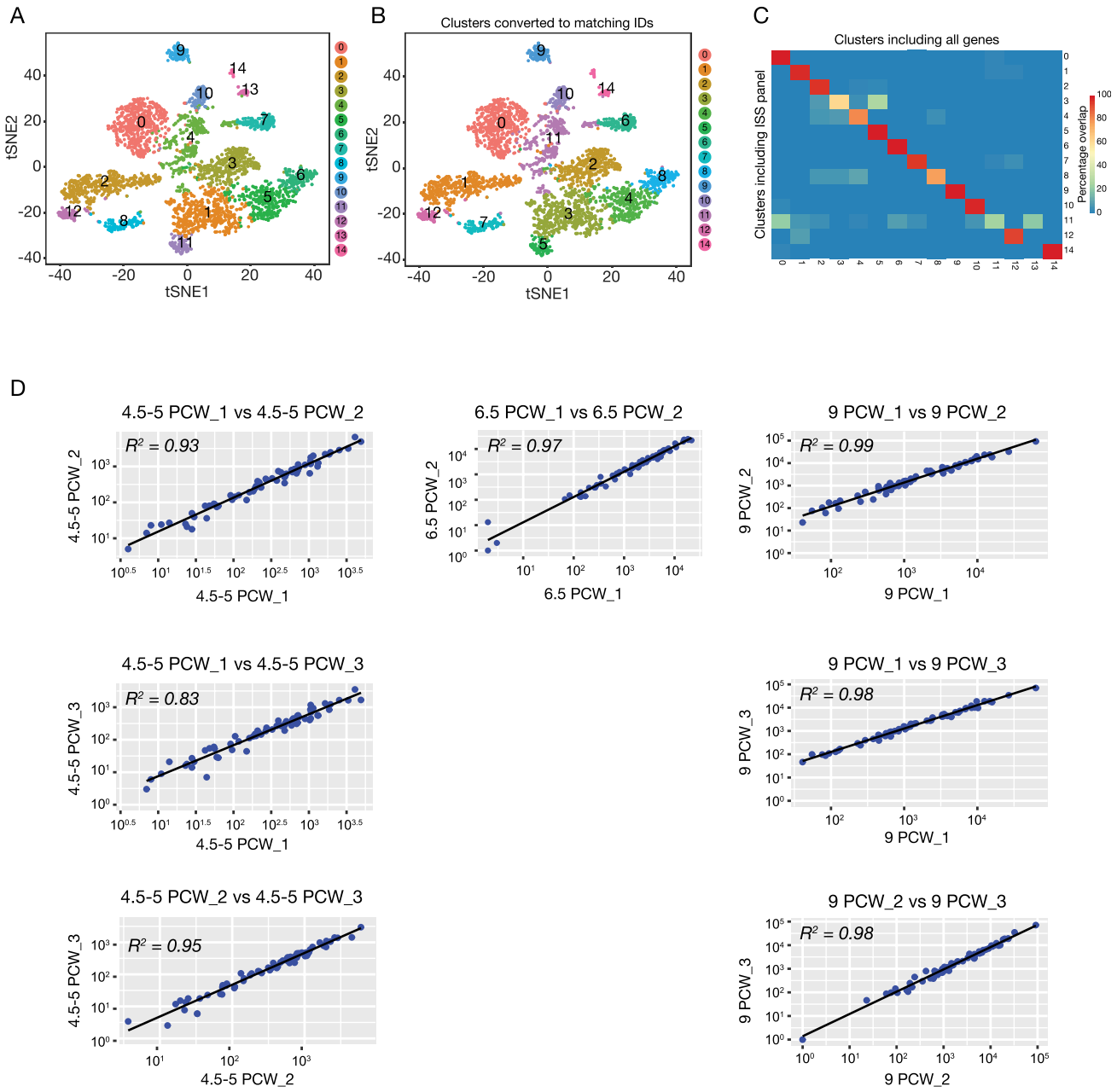

Figure S4. *In Situ* Sequencing Experimental Features, Related to Figure 5

(A) Dimensionality reduction and clustering of the scRNA-seq data based only on the 69 genes included in the ISS panel.

(B) tSNE plot as in (A) with cluster numbers converted to matching IDs and colors as in Figure 3B based on their percentage of overlap.

(C) Heatmap showing the percentage of overlap. Percentages are calculated as the number of cells in a 69-gene cluster divided by the total number of cells in the best matching original cluster. Original cluster 13 (immune cells) is not seen in the 69-gene cluster formation as no markers were designed for it.

(D) Correlations among tissue sections of the same developmental time point. Analyses are based on the gene expression of all genes included in the gene panel. 4.5-5 PCW_1, 4.5-5 PCW_2 and 4.5-5 PCW_3 indicate three tissue sections from the 4.5-5 PCW heart; 6.5 PCW_1, and 6.5 PCW_2 indicate two tissue sections from the 6.5 PCW heart; 9 PCW_1, 9 PCW_2 and 9 PCW_3 are three tissue sections from the 9 PCW heart. To check goodness-of-fit measure for linear regression models, R-square, coefficient of determination is applied. Value = 1 indicates that the model explains all the data around its mean.

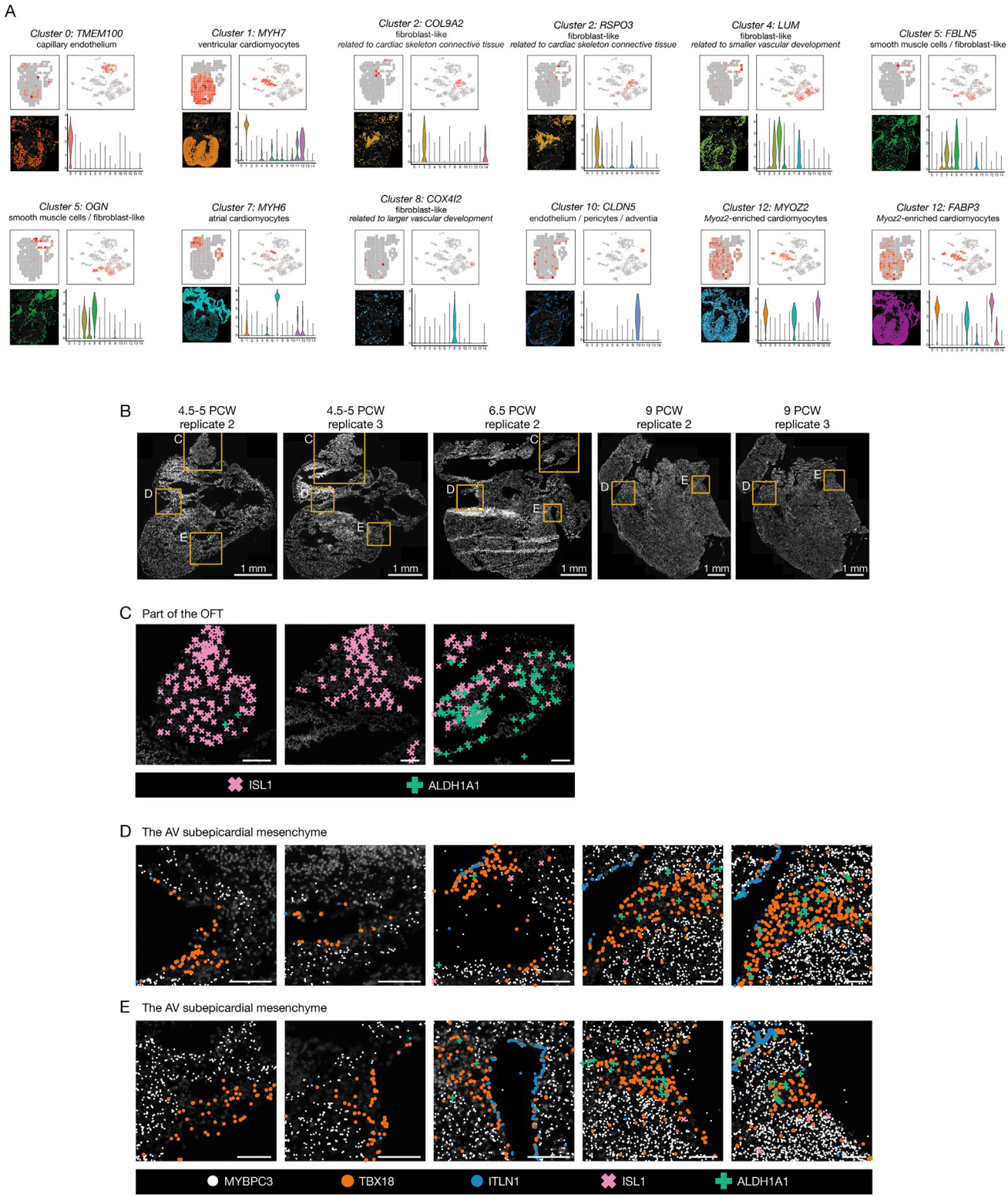

Figure S5. Gene Expression across Heart Development, Related to Figure 6

(A) Twelve marker genes included the ISS gene panel showing their gene expression patterns in a heatmap across ST tissue sections and scRNA-seq tSNE plot, in a violin plot throughout scRNA-seq clusters, and as registered transcripts in ISS tissue sections.

(legend continued on next page)

(B) Overview of technical replicates of the tissue sections shown in Figure 6C. Yellow squares indicate tissue domains that are magnified and showed in (C-E). Scale bar, 1 mm.
(C) Magnified images of the OFT domain in the 4.5-5 PCW and 6.5 PCW replicates, showing an identical pattern as seen in Figure 6D. The two replicates of 9PCW tissue section did not contain this region. Scale bar, 200 μm.
(D-E) Magnified images of the right (D) and left (E) AV subepicardial mesenchyme domain in the replicates of all three time points, showing identical patterns as seen in Figures 6E–6F. Scale bars, 200 μm.
(A–E) Figures contain tiled images to cover the entire tissue.

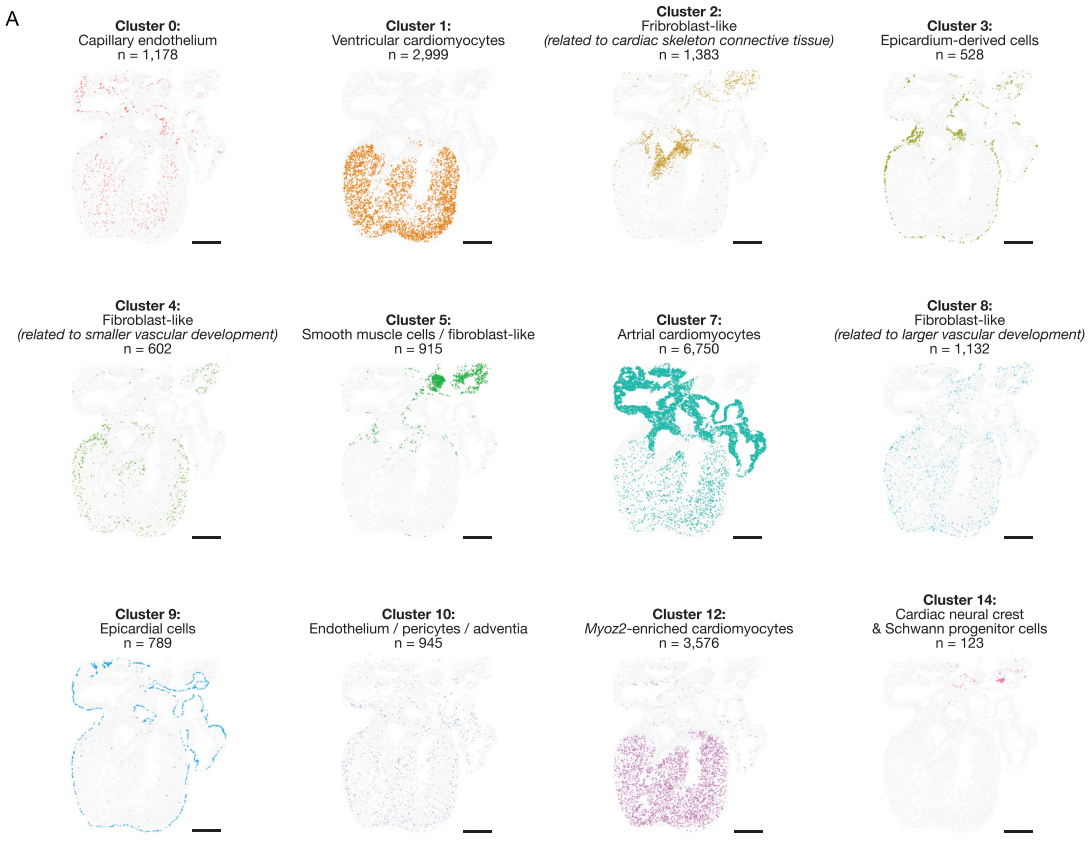

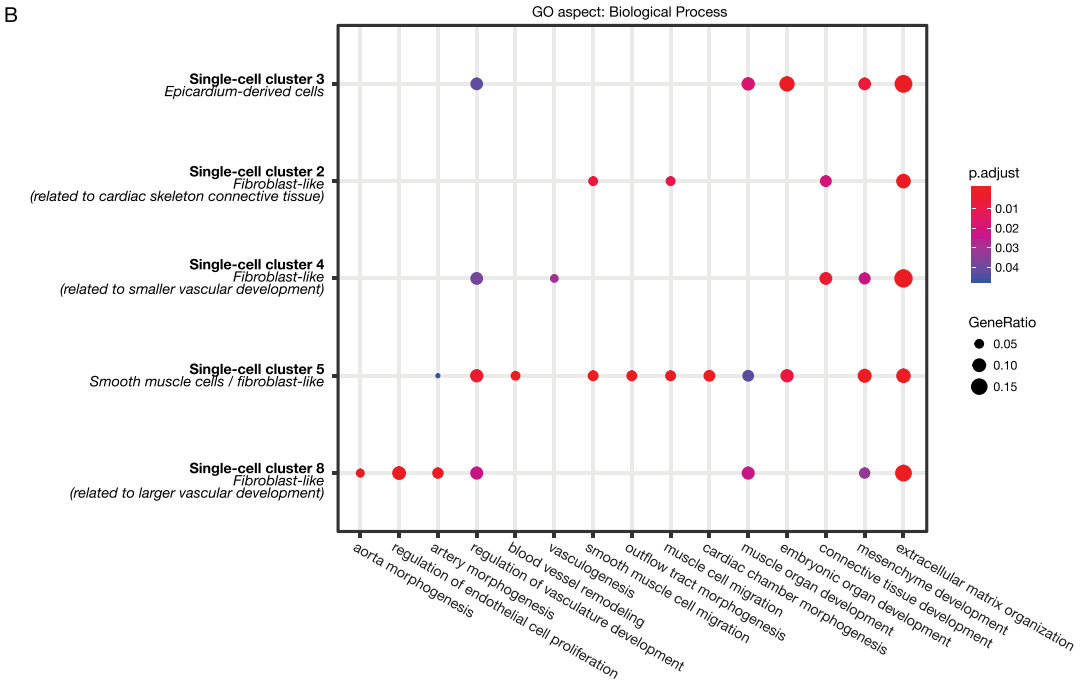

(legend on next page)

Figure S6. Spatial Distribution and Features of Individual Cell Clusters in the 6.5 PCW Heart, Related to Figure 6

(A) The probabilistic cell map was obtained using pciSeq (Qian et al., 2019). Each dot represents a single cell shown as a pie chart of probabilities matching to scRNA-seq clusters. Cell cluster are named and color-coded according to Figure 3B, and number of identified single cells of each cluster are listed. A threshold of at least five reads per cells was set. Scale bars, 100 μm.

(B) Gene ontology annotations of upregulated genes with adjusted p value lower than 0.05 across heart biological processes. The dots in the dotplot indicate the GO categories in which ST clusters are more likely to have biological meaning. The color of dots indicates high (red) or low (blue) enrichment for a specific GO category. The size of dots displays the overlap between the input gene lists with the collection of gene sets.

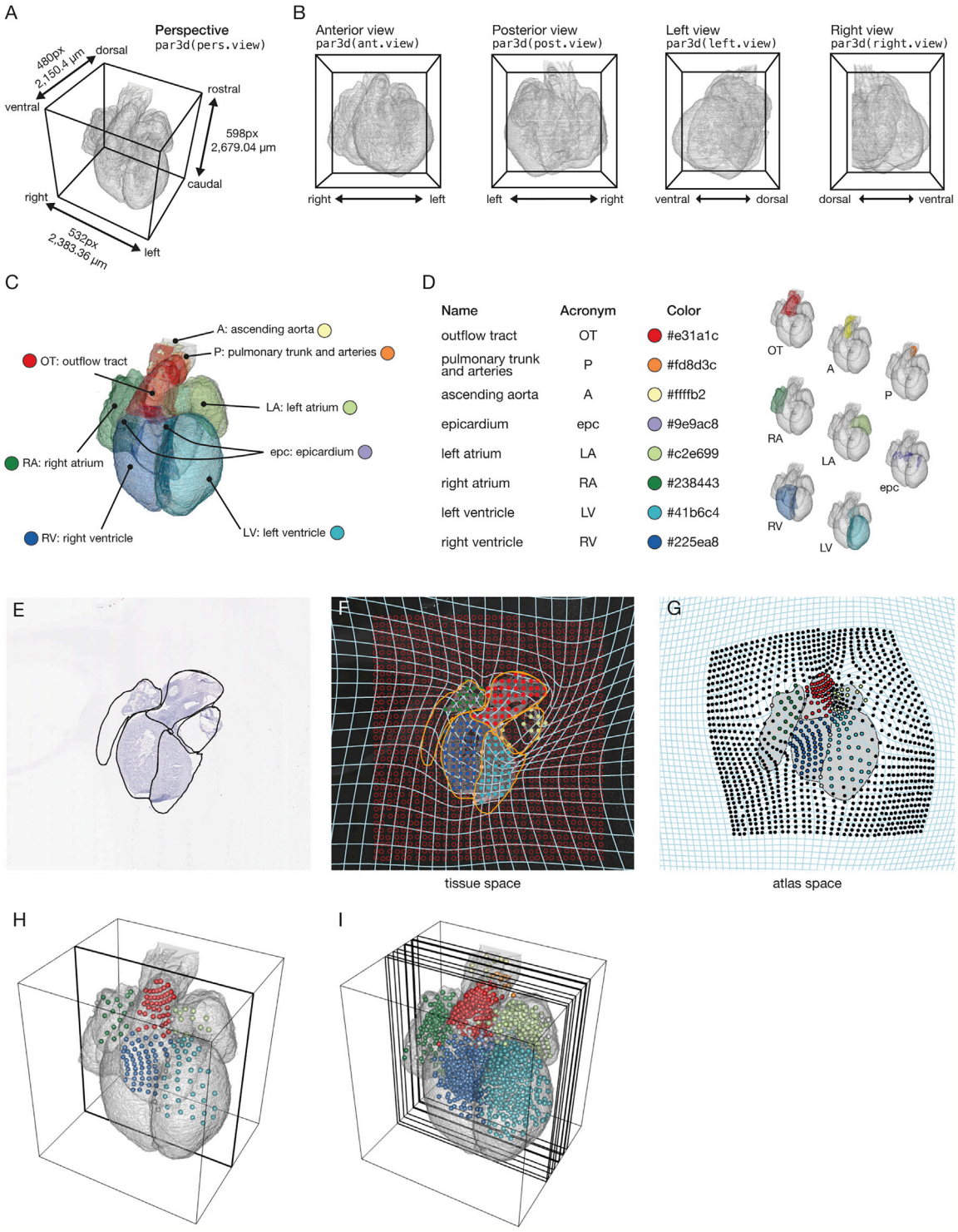

Figure S7. Construction of a 3D Model of the Developing Human Heart, Related to Figure 7

(A) 3D visualization of the developing human heart (Carnegie stage 18).

(B) 3D visualization with anterior, posterior, left, and right views.

(C) The eight anatomical regions of the heart atlas.

(D) Specifications of each anatomical region, as well as its position within the heart atlas.

(E) Example of a bright field image from one tissue section of the 6.5 PCW heart, with the black lines delimiting the anatomical regions within the atlas.

(legend continued on next page)

(F) The positions of spots are visualized in tissue space.
(G) The positions of spots are visualized in atlas space.
(H) The positions of spots are visualized in the context of the entire atlas.
(I) The positions of all spots from nine tissue sections of the 6.5 PCW heart sample.